Author/s:
Hu, Y;Cortez-Jugo, C;Ju, Y;Zheng, T;Zhou, J;Lin, Z;De Rose, R;Hagemeyer, CE;Alt, K;Caruso, F

Title:
Poly(ethylene glycol) Cross-Linked Antibody Nanoparticles for Tunable Biointeractions

Date:
2023

Citation:
Hu, Y., Cortez-Jugo, C., Ju, Y., Zheng, T., Zhou, J., Lin, Z., De Rose, R., Hagemeyer, C. E., Alt, K. & Caruso, F. (2023). Poly(ethylene glycol) Cross-Linked Antibody Nanoparticles for Tunable Biointeractions. Chemistry of Materials, 35 (13), pp.4965-4978. https://doi.org/10.1021/acs.chemmater.3c00323.

Poly(ethylene glycol) Cross-Linked Antibody Nanoparticles for Tunable Biointeractions

*Yingjie Hu,[a] Christina Cortez-Jugo,[a] Yi Ju,[a,b] Tian Zheng,[c] Jiajing Zhou,[a] Zhixing Lin,[a] Robert De Rose,[a] Christoph E. Hagemeyer,[d] Karen Alt,[d] and Frank Caruso[a]**

[a]Department of Chemical Engineering, The University of Melbourne, Parkville, Victoria 3010, Australia

[b]School of Health and Biomedical Sciences, RMIT University, Bundoora, Victoria 3083, Australia

[c]Materials Characterisation and Fabrication Platform, Department of Chemical Engineering, The University of Melbourne, Parkville, Victoria, 3010, Australia

[d]Australian Centre for Blood Diseases, Central Clinical School, Monash University, Melbourne, Victoria 3004, Australia

*Corresponding author. E-mail: fcaruso@unimelb.edu.au

ABSTRACT

Liver accumulation of nanoparticles is a major challenge in nanoparticle-mediated delivery, as it can reduce the delivery of the nanoparticles to their intended site and lead to liver damage and

toxicity. Recent studies have shown that particle engineering, e.g., nanoparticle composition, can influence liver uptake and allow homing of nanoparticles to specific organs or tissues. Herein, we investigated the role of nanoparticle cross-linking on liver uptake. We developed a series of antibody nanoparticles (AbNPs) using various poly (ethylene glycol) (PEG) molecule (e.g., different arm numbers and arm lengths) cross-linkers. Specifically, AbNPs based on Herceptin were engineered with PEG cross-linker architectures ranging from 2-arm (at molecular weights of 600 Da, 2.5 kDa, and 5 kDa) to 4-arm, and 8-arm via a mesoporous silica templating method. The molecular architecture of PEG modulated not only the targeting ability of the AbNPs in model cell lines, but also their interaction with phagocytes in human blood. Increasing the PEG arm length from 600 Da to 5 kDa also reduced the uptake of the nanoparticles in the liver by 85%. Tumor accumulation of Herceptin AbNPs cross-linked with a 5 kDa 2-arm-PEG was 50% higher compared with control AbNPs and displayed similar liver uptake as free Herceptin. This study highlights the role of PEG cross-linking on receptor targeting and liver uptake, which influence tumor targeting, and combined with the versatility and multifunctionality of the antibody nanoparticle platform could lead to the development of organ-selective targeted antibody nanoparticle assemblies.

INTRODUCTION

The intravenous injection of nanoparticles typically results in their accumulation in the liver, often via sequestration by liver-resident macrophages called Kupffer cells. Premature liver uptake of nanoparticles results in their reduced capacity to reach their target site, including tumors, and potential liver damage and hepatic cellular toxicity. Strategies to overcome liver uptake have been investigated, including at the physiological level by either removing Kupffer cells[1] or preloading Kupffer cells with nonactive nanomaterials.[2,3]

Recent studies have shown that varying nanoparticle composition can drive the homing of nanoparticles to organs or tissues other than the liver.[4–6] A widely applied approach to reduce liver uptake and prolong circulation time has been to functionalize nanoparticles with poly(ethylene glycol) (PEG), commonly known as PEGylation.[7–9] PEG provides nanoparticles with stealth properties by forming a hydration layer that hinders significant protein adsorption and reduces uptake by the phagocytic cells.[10–15] The effects of PEG surface density, molecular weight, and branching (arm number) on the stealth properties of PEGylated nanoparticles have been widely studied using a range of nanoparticle systems and biomacromolecules.[8,16–21]

A limitation of PEG is that it can reduce membrane interactions at the cellular level and limit the biological activity of functional molecules.[19] This limitation has been attributed to the low-fouling nature of PEG and possible steric crowding at the active or binding site.[22–25] Specifically, when conjugated on either antibodies or antibody-functionalized nanoparticles, PEG can hinder the specific binding of the antibody to its antigen, which could be on the cell surface.[24] Despite the extensive studies on PEGylation, there is no general criterion as to what is essential to balance the stealth and biological activities of PEGylated nanoparticles due to the physicochemical differences among the particles systems used in these studies.[17,18,22,23,26–30] For PEGylated antibody-targeted nanoparticles, specifically, it is important to understand how PEGylation affects the specific antibody–receptor binding to achieve optimal targeting and stealth abilities. For instance, a study on targeted liposomes showed that the antibody ligand has to be sufficiently longer (at least twice) than the neighboring PEG on the particle surface.[31] A study involving PEG chains on poly(lactic-*co*-glycolic acid) nanoparticles has also shown that the efficiency of nanoparticle binding on dendritic cells is higher at shorter PEG lengths (molecular weight (M_w) 3000 g mol^{-1}) than at longer PEG lengths (M_w > 6000 g mol^{-1}).[32]

We recently reported the mesoporous silica template-assisted assembly of ~200 nm antibody nanoparticles (AbNPs) that were cross-linked with poly(ethylene glycol)-*N*-hydroxysuccinimide (PEG-NHS, M_w 600 Da).[33] The AbNPs could be synthesized with controlled size and composition and exhibited promising features for biomedical applications, including the selectivity of the monoclonal antibody to recognize its target on the cell membrane, which triggered downstream cellular events (arrest in cell proliferation). When injected intravenously, the AbNPs accumulated mostly in the liver. To achieve the desired targeting action of the AbNPs, it is essential to improve their stealth properties and reduce liver uptake. In the present study, various PEG cross-linkers with different arm lengths and arm numbers were used to prepare PEGylated antibody nanoparticles (designated as PEG*x*-AbNPs, where *x* denotes the total PEG M_w and Ab is the antibody e.g., Herceptin (Her)) via the mesoporous silica template-assisted assembly platform. Using Herceptin (or trastuzumab) as the model antibody, assembly, selective targeting, phagocytic association in human blood, and biodistribution in mice of the PEG*x*-AbNPs were investigated to gain a fundamental understanding of the influence of PEG cross-linker molecular architecture (i.e., arm length and arm number) on the in vitro, ex vivo, and in vivo bio–nano interactions of antibody nanoparticles. While the study uses Herceptin as a model in the material assembly, the wide applicability of monoclonal antibodies for applications beyond tumor targeting and against intracellular targets could lead to multifunctional antibody assemblies for a range of applications.

EXPERIMENTAL SECTION

Materials. Cetyltrimethylammonium bromide (CTAB), tetraethyl orthosilicate (TEOS), triethanolamine (TEA), sodium salicylate (NaSal), hydrofluoric acid (HF; 48 wt%), ammonium fluoride (NH_4F), sodium carbonate (Na_2CO_3), dimethyl sulfoxide (DMSO), phenazine methosulfate (PMS), glutathione (GSH), 3-(N-morpholino)propanesulfonic acid (MOPS),

immunoglobulin G (IgG) from sheep serum, and proteinase K from *Tritirachium album* were purchased from Sigma-Aldrich. PEG-NHS (2-arm-PEG-NHS: M_w 600 Da, 2.5 kDa, and 5 kDa) were purchased from Creative PEGworks. Multi-arm PEG-NHS (4-arm-PEG-NHS: M_w 5 kDa; 8-arm-PEG-NHS: M_w 10 kDa) were purchased from Jenkem. Alexa Fluor 488 carboxylic acid succinimidyl ester (AF488), Alexa Fluor 647 carboxylic acid succinimidyl ester (AF647), RPMI 1640 medium, Dulbecco's modified Eagle's medium (DMEM), fetal bovine serum (FBS), Dulbecco's phosphate-buffered saline (DPBS) buffer, Alexa Fluor 594-wheat germ agglutinin conjugate (AF594-WGA), trihydrochloride (Hoechst 33342), and 2,3-bis[2-methoxy-4-nitro-5-sulfophenyl]-2*H*-tetrazolium-5-carboxyanilide inner salt (XTT) were purchased from Thermo Fisher Scientific. Tris/glycine/sodium dodecyl sulfate running buffer and 4–20% Mini-PROTEAN TGX stain-free protein Bis-Tris gels were purchased from Bio-Rad. NuPAGE LDS sample buffer and SeeBlue Plus2 prestained protein standard were purchased from Thermo Fisher Scientific. Thulium(III) *S*-2-(4-isothiocyanatobenzyl)-1,4,7,10-tetraazacyclododecane-1,4,7,10-tetraacetic acid (Tm-*p*-SCN-Bn-DOTA) was purchased from Macrocyclics. 2,5-Dioxopyrrolidin-1-yl 5-(8-methyl-3,6,10,13,16,19-hexaaza-bicyclo[6.6.6]icosan-1-ylamino)-5-oxopentanoate (MeCOSar-NHS) was synthesized as previously described.[34] Herceptin antibodies were from F. Hoffmann-La Roche Ltd. Ultrapure water with a resistance of greater than 18 MΩ cm (Milli-Q water) was obtained from a three-stage Millipore Milli-Q Plus 185 purification system.

Preparation of Antibody Nanoparticles. Mesoporous silica nanoparticle (MSN) templates with large pores were synthesized via the anion-assisted method using CTAB as a cationic surfactant, NaSal as a structure-directing agent, TEOS as a silica source, and TEA as a catalyst, as described in previous studies.[33] Briefly, 68 mg TEA, 380 mg CTAB, and 168 mg NaSal were successively added to 25 mL Milli-Q water, and the mixture was stirred at 80 °C in an oil bath for

1 h. Afterwards, 4 mL TEOS was slowly added to the above solution and stirred at 80 °C for 2 h. The products were collected by centrifugation at 10000 *g* and washed three times with ethanol. The products were then purified by extraction with ~1 M HCl in methanol at 60 °C for 6 h; the extraction process was repeated three times. The MSNs were washed with ethanol and finally oven-dried at 80 °C overnight.

Subsequently, 500 µL Herceptin solution (2 mg mL^{-1}) was added to 500 µL MSN solution (2 mg mL^{-1}) in sodium acetate buffer (0.1 M, pH 5.0). The particle/protein dispersion was allowed to incubate for 2 h at room temperature on an Eppendorf thermomixer to allow the antibody molecules to infiltrate the pores of the templates via electrostatic adsorption. Excess antibodies were removed by centrifugation (~5000 *g*, 5 min, ×3), and the Herceptin-loaded nanoparticles were dispersed in DPBS (pH 7.4). The PEG-NHS cross-linker with different arm lengths or arm numbers in DMSO (e.g., 50 µL of 20 mg mL^{-1} of PEG-NHS cross-linker) was added to the Herceptin-loaded MSNs in PBS buffer and allowed to incubate for 4 h at room temperature with constant agitation. The molar ratio of NHS functional groups to antibody molecules was kept consistent at 500:1 for all samples. PEG*x*-HerNPs were finally obtained by dissolving the MSN template with 1 M HF/3 M NH_4F solution (pH ~5), followed by washing with DPBS buffer three times. *Caution! HF is highly toxic. Extreme care should be taken when handling HF solution, and only small quantities should be prepared.* Nonspecific control particles IgGNPs were prepared following the same methods but IgG from sheep serum was used instead of Herceptin.

PEG-NHS with different arm lengths (2-arm-PEG-NHS with M_w 600, 2.5k and 5k) and PEG-NHS with different arm numbers (2-, 4- and 8-arm-PEG-NHS, with M_w 2.5k, 5k and 10k) are respectively denoted as 2-arm-PEG(600)-NHS, 2-arm-PEG(2.5k)-NHS, 2-arm-PEG(5k)-NHS, 4-arm-PEG(5k)-NHS, and 8-arm-PEG(10k)-NHS. The term PEG*x*-AbNPs is used to describe the

PEGylated antibody nano-assemblies collectively and include 2-arm-PEG(600)-AbNPs, 2-arm-PEG(2.5k)-AbNPs, 2-arm-PEG(5k)-AbNPs, 4-arm-PEG(5k)-AbNPs, and 8-arm-PEG(10k)-AbNPs.

Antibody Labeling. For antibody labeling, 5 μL AF488 or AF647 (1 mg mL^{-1}) in DMSO was added to 200 μL antibody solution (5 mg mL^{-1}) in DPBS containing 0.1 M Na_2CO_3 (pH 8.3) for 2 h at room temperature with constant agitation. Excess free fluorophores were removed using Zeba™ spin desalting columns (40 kDa molecular weight cutoff, 2 mL). The labeled antibodies were then used to prepare fluorescently labeled PEG*x*-AbNPs (see above) to facilitate fluorescence-based analysis. As the incubation of labeled antibodies with templates and the molar ratio of NHS group:Ab were consistent between all particles, it is assumed that all particles have the same antibody loading efficiency and hence similar particle fluorescence.

Particle Characterization. The concentration of Herceptin in 2-arm-PEG(600)-HerNPs was determined using a Pierce BCA protein assay kit; particle concentration was measured by nanoparticle tracking analysis using a 405 nm laser (Nanosight NS300, Malvern Panalytical, UK). Transmission electron microscopy (TEM) images were taken on an FEI Tecnai Spirit microscope operated at 120 kV. Samples were prepared by placing a drop of a sample suspension (suspended in deionized water) on a carbon-coated copper grid and drying under ambient conditions. Hydrodynamic size distribution and ζ-potentials were measured using a Zetasizer Nano ZS (Malvern Instruments, UK). Atomic force microscopy (AFM) images were acquired using a Cypher ES atomic force microscope (Asylum Research, USA). Circular dichroism (CD) spectra were recorded on a circular dichroism spectrometer (Model 401, AVIV Biomedical, USA). Fourier transform infrared (FTIR) spectra in attenuated total reflectance mode were recorded using an FTIR spectrometer (TENSOR II, Bruker, Germany).

Stability in GSH and Proteinase. Free Herceptin and PEG*x*-HerNPs were incubated in 5 mM GSH or 1 mg mL^{-1} proteinase in DPBS for 24 h under constant agitation. After incubation, the degradation profiles of PEG*x*-HerNPs were determined by sodium dodecyl sulfate polyacrylamide gel electrophoresis (SDS-PAGE). Briefly, each sample was added to NuPAGE LDS sample buffer and heated to 70 °C for 10 min. SeeBlue Plus2 prestained protein standard and an aliquot of 15 μL per sample were loaded on a Bio-Rad 4−20% Mini-PROTEAN TGX stain-free gel to run at 120 V for 30 min. Gels were imaged under UV irradiation using a Bio-Rad Gel documentation XR system.

Quantitative Degradation Profiles in Proteinase. AF488-labeled free Herceptin antibody or PEG*x*-HerNPs were dispersed in 1 mL proteinase solution (1 mg mL^{-1} in DPBS) and contained in a dialysis tubing with a molecular weight cutoff of 100 kDa. The dialysis tubing was further incubated in an external chamber filled with 9 mL proteinase solution (1 mg mL^{-1}) under constant agitation. The same protocol was repeated in DPBS as control. After incubation for 2, 4, 6, 8, 10, 24, or 48 h, the AF488 fluorescence intensity in the external chamber solution ($I_{degraded}$) was determined using an Infinite M200 microplate reader (Tecan, Switzerland). The same amount of AF488-labeled Herceptin or PEG*x*-HerNPs was dispersed in 10 mL protease solution (1 mg mL^{-1}) and their corresponding AF488 fluorescence intensity (I_{total}) was measured using the microplate reader. The degradation percentage of each sample at different time points was calculated as follows: Degradation (%) = $I_{degraded}/I_{total} \times 100\%$.

Cell Culture. ErBb2+ human breast cancer BT-474 cells were maintained in RPMI medium 1640 supplemented with 10% (v/v) FBS. ErbB2− human breast cancer MDA-MB-231 cells and Raw 267.4 macrophage cells were grown in DMEM with 10% (v/v) FBS. All cultures were

maintained at 37 °C in a 5% CO_2-humidified atmosphere. Cells at passages 3–10 were used in this experiment.

Cellular Association Assessed by Flow Cytometry. Cells were seeded at a density of 10^5 per well in a 24-well plate and incubated at 37 °C overnight. Then, the culture medium was removed and replaced with fresh medium containing AF488-labeled free Herceptin antibody or PEG*x*-HerNPs. The dosage was kept consistent at 20 μg mL^{-1} protein for all antibody and particle samples, as measured using UV–vis spectrophotometry (NanoDrop™, Thermo Fisher Scientific) and a microBCA protein quantification assay according to the manufacturer's instructions (Pierce Micro BCA Protein Assay Kit, Thermo Fisher Scientific). A dosage of 20 μg mL^{-1} per 10^5 cells is at saturating levels,[35] and keeping the protein concentration consistent for the free antibody and PEG*x*-AbNPs samples ensures the same amount of fluorescent antibody in each sample. After incubation for various time periods (1, 3, 6, 12, or 24 h), cells were gently washed with DPBS to remove unassociated nanoparticles, followed by treatment with 0.25% trypsin at 37 °C for 5 min. The cells were collected via centrifugation at 300 *g* for 5 min and the resulting pellet was then resuspended in DPBS. Finally, the cells were analyzed on an Apogee A50-Micro flow cytometer. At least 10^4 cells were analyzed for each sample.

Cellular Internalization Assessed by Imaging Flow Cytometry. Cells were seeded in a 6-well plate at a density of 5×10^5 cells per well and incubated overnight. Then, the culture medium was removed and replaced with fresh medium containing AF488-labeled free Herceptin or PEG*x*-HerNPs (20 μg mL^{-1}). After 24 h of incubation, cells were washed gently with DPBS, harvested with 0.25% trypsin, and collected via centrifugation at 300 *g* for 5 min. The resulting pellet was then resuspended and fixed in 200 μL 4% paraformaldehyde for 15 min at room temperature. Following this, cells were incubated with AF594-WGA (5 μg mL^{-1}) for 5 min at room temperature

to stain the membrane, then further washed twice with DPBS and resuspended in 100 µL DPBS. Finally, cells were analyzed using an AMNIS ImageStream®^{X} Mark II imaging flow cytometer (Amnis Corporation, USA). At least 5000 cells were analyzed for each sample. The built-in internalization wizard of Amnis ImageStream IDEAS software was used to calculate the internalization percentage on focused single cells statistically.

Cellular Internalization Assessed by Confocal Microscopy. Cells were seeded in an 8-well Lab-Tek II chambered slide at a density of 5×10^4 cells per well for 24 h. After incubation, cells were treated with AF488-labeled free Herceptin or PEG*x*-HerNPs (20 µg mL^{-1}) for 24 h. Then, the cells were washed with DPBS, fixed with 4% paraformaldehyde for 15 min at room temperature, stained with AF594-WGA for 5 min, and counterstained with Hoechst 33342 for another 5 min. The cells were washed with DPBS after each staining step and finally immersed in DPBS before imaging on a Nikon A1R+ confocal microscope.

Cell Proliferation. Cells were seeded at a density of 1×10^4 cells per well in triplicate in 96-well microplates and allowed to adhere overnight. Free Herceptin or PEG*x*-HerNPs were added and incubated with cells for 48 h. For all samples, the concentration of the antibody was kept constant at 20 µg mL^{-1}. After incubation, the culture medium was replaced by fresh medium containing 0.2 mg mL^{-1} of activated XTT (10 mL of 0.2 mg mL^{-1} XTT in complete medium was activated by adding 20 µL of 1 mM PMS in DPBS), and cells were allowed to incubate further at 37 °C for 3 h. Cell viability was measured using the microplate reader at 475 nm, with 675 nm as the reference wavelength. Cell viability is expressed as a percentage by normalizing against the absorbance of untreated cells.

Association with Phagocytes from Human Whole Blood. Fresh blood was collected from healthy human volunteers into VACUETTE sodium heparin tubes (Greiner Bio-One) after

obtaining informed consent in accordance with The University of Melbourne Human Ethics Approval #1443420 and the Australian National Health and Medical Research Council (NHMRC) National Statement on Ethical Conduct in Human Research. AF647-labeled free Herceptin or PEG*x*-HerNPs (2 μg) were incubated in 100 μL whole blood at 37 °C for 1 h. Subsequentially, the samples were treated with lysing buffer (BD Pharm Lyse) following the manufacturer's protocol to lyse red blood cells. The remaining blood cells were further washed with flow cytometry staining (FCS) buffer at 500 *g* for 7 min and resuspended in 100 μL FCS buffer. Fluorophore-conjugated antibodies (titrated concentration) against CD56 (natural killer (NK) cells), CD19 (B cells), CD66b (neutrophils), HLA-DR (dendritic cells; HLA-DR+ (CD3, CD19, CD14, CD56)−), CD3 (T cells), or CD14 (monocytes) were added and incubated for 1 h on ice. Unbound antibodies were removed by washing twice with cold (4 °C) FBS buffer (500 *g*, 7 min). Cells were fixed with 2% w/v formaldehyde in PBS and directly analyzed by flow cytometry (CytoFLEX, Beckman Coulter Life Sciences), and data were processed using FlowJoV10.

Biodistribution in Mice. Tm-labeled PEG*x*-HerNPs were prepared by conjugating Tm-*p*-SCN-Bn-DOTA with the Herceptin antibodies. Briefly, 27.7 μL Tm-*p*-SCN-Bn-DOTA (10 mg mL^{-1}) in DMSO was added to 2 mL antibody solution (5 mg mL^{-1}) in 0.1 M $NaHCO_3$ buffer (pH 9) for 2 h at 37 °C with constant agitation. Excess Tm-*p*-SCN-Bn-DOTA was removed using Zeba spin desalting columns (40 kDa molecular weight cutoff, 2 mL). The labeled antibodies were then used to prepare Tm-labeled PEG*x*-HerNPs.

All biodistribution procedures were conducted in accordance with the Australian code for the care and use of animals for scientific purposes, and experiments were approved by The University of Melbourne Animal Ethics Committee (10404). Mice were sourced from the Animal Resources Centre (Perth, Australia) and housed on a 12 h light/dark cycle with ad libitum access to food and

water. The biodistribution of Tm-labeled PEG*x*-HerNPs was studied in 6–7-week-old healthy female BALB/c mice. The mice were randomly divided into groups of 3 mice. A group of mice were injected intravenously with Tm-labeled PEG*x*-HerNPs (1 mg mL^{-1}) or Tm-labeled free Herceptin antibody (1 mg mL^{-1}) at a dosage at 10 mg kg^{-1} via the lateral tail vein. A blood sample was drawn at 4 h after administration, and the mice were subsequently euthanized, and the blood removed from organs by intracardial perfusion with DPBS. The organs of interest were harvested, weighed, and digested with 2 mL of 60% nitric acid at 70 °C for 2 h. *Caution! Extreme care should be taken when handling 60% nitric acid, which can only be used in a fume hood.* Tm signal in the blood and organ samples was measured by ICP-MS.

Targeting in Tumor-Bearing Mice. *Preparation of Chelator–AbNPs:* MeCOsar-conjugated free antibody and AbNPs (2-arm-PEG(5k)-HerNPs and 2-arm-PEG(5k)-IgGNPs) were prepared to allow for ^{64}Cu labeling. Briefly, 5 µL MeCOsar-NHS[34,36] (1 mg mL^{-1}) in DMSO solution was added to 1 mL antibody solution (5 mg mL^{-1}) in MOPS buffer (20 mM, pH 7), and the mixture was incubated for 1 h at 37 °C with constant agitation (400 rpm on a ThermoMixer). Excess MeCOsar-NHS was removed using Zeba spin desalting columns (40 kDa molecular weight cutoff, 2 mL). The conjugated antibodies were then used to prepare MeCOsar-conjugated AbNPs.

^{64}Cu Radiolabeling of Chelator–AbNPs: The MeCOsar-conjugated free antibodies (Herceptin, IgG) and AbNPs (2-arm-PEG(5k)-HerNPs and 2-arm-PEG(5k)-IgGNPs) were incubated with 10 MBq of ^{64}Cu (Austin Hospital) per 10 µg protein in 0.1 M pH 7.4 MOPS buffer for 20–30 min at room temperature.[34,37] Samples of each solution were taken and mixed with 10 µL of 50 mM diethylenetriamine pentaacetate for 5 min. Unbound ^{64}Cu was removed by purification using 30 kDa molecular weight cutoff spin columns (Thermo Fisher Scientific) as per manufacturer's protocols. All samples showed >95% labeling.

Preparation of Subcutaneous Xenograft Tumor in Mice: All tumor targeting procedures were conducted in accordance with the Australian NHMRC's published Code of Practice for the Use of Animals in Research, and experiments were approved by the Alfred Medical Research and Education Precinct Animal Ethics Committee (E/1697/2016/M). Six-week-old female BALB/c nu/nu mice were purchased from the Animal Resources Centre (Perth, Australia) and housed on a 12 h light/dark cycle with ad libitum access to food and water.

SK-OV-3 cells (2.5×10^6 in 100 μL Matrigel and 100 μL PBS) were used to inoculate a subcutaneous tumor on the right shoulder of each female nude mouse. The body weight and tumor volume were monitored twice a week. The tumor diameter (D) was measured, and the corresponding tumor volume was calculated using the following formula: volume = $(4/3)\pi(D/2)^3$. The xenograft tumor-bearing mice were randomized into two groups after 2 weeks of tumor growth (tumor size up to 400 mm^3) for positron emission tomography (PET) imaging.

PET Imaging: ^{64}Cu-labeled free antibodies, 2-arm-PEG(5k)-HerNPs, or 2-arm-PEG(5k)-IgGNPs were injected via the tail vein (29G needle, 10 μg protein / 5–7 MBq). At 24 h postinjection, positron emission tomography/computed tomography (PET/CT) was performed using a NanoPET/CT in vivo preclinical imager (Mediso Ltd., Budapest, Hungary) with a 30 min PET acquisition time and a coincidence relation of 1–3. Image reconstruction was performed with the following parameters: OSEM with SSRB 2D LOR, energy window, 400–600 keV; filter Ramlak cutoff 1, number of iterations/subsets, 8/6. The radioactivity accumulation in various organs was calculated based on the PET images via a volume of interest and displayed as kBq cc^{-1}.

Minimum Information Reporting in Bio–Nano Experimental Literature (MIRIBEL). The studies conducted herein, including material characterization, biological characterization, and

experimental details, conform to the MIRIBEL reporting standard for bio–nano research,[38] and we include a companion checklist of these components in the Supporting Information.

RESULTS AND DISCUSSION

Synthesis and Characterization of PEG*x*-AbNPs. The synthesis of PEG*x*-AbNPs is shown in Scheme 1. Using a template-assisted antibody assembly method we reported previously[33] antibodies were loaded in MSN templates followed by cross-linking with various PEG-NHS (PEG*x*-NHS) linkers and removal of the MSN template to obtain PEG*x*-AbNPs. MSN templates with large pores (~20 nm in diameter)[33,39] were synthesized to accommodate the antibodies, which have dimensions of approximately 14.5 nm × 8.5 nm × 4.0 nm.[40] Incubation with PEG-NHS cross-links the antibodies that are present in the pores and surface of the particles by amide bond formation with the amine groups on IgG. To study the effect of PEG cross-linking on bio–nano interactions, in this study, PEG-NHS with different arm lengths (2-arm-PEG-NHS with M_w 600, 2.5k and 5k) and PEG-NHS with different arm numbers (2-, 4- and 8-arm-PEG-NHS, with M_w 2.5k, 5k and 10k, respectively) were used for cross-linking to prepare the PEG*x*-AbNPs (PEGylated antibody nano-assemblies). These nano-assemblies include 2-arm-PEG(600)-AbNPs, 2-arm-PEG(2.5k)-AbNPs, 2-arm-PEG(5k)-AbNPs, 4-arm-PEG(5k)-AbNPs, and 8-arm-PEG(10k)-AbNPs.

Scheme 1. Synthesis of PEG*x*-AbNPs Cross-Linked by Various PEG Linkers.[a]

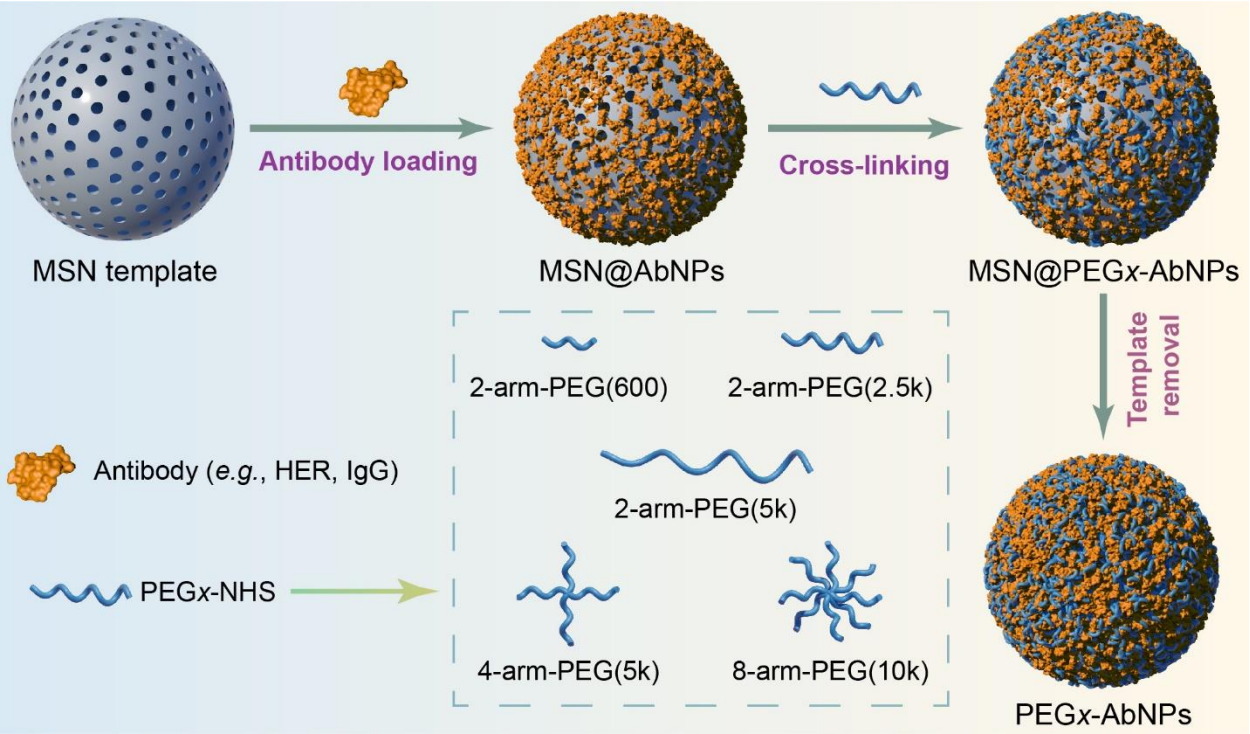

[a]As an example, Herceptin antibodies can be loaded in an MSN template followed by cross-linking with various PEG-NHS (PEG*x*-NHS) and removal of the MSN template.

Antibody loading in the MSN templates has been estimated to be ~700 μg IgG protein mg^{-1} of MSN (~70% loading efficiency) or approximately 3.58×10^4 IgG molecules per particle after template removal, as we reported previously.[33] To enable the functional characterization of the PEG*x*-AbNPs, Herceptin was used as a model IgG antibody, although this assembly method is applicable to other IgG-type monoclonal antibodies and even antibody–drug conjugates;[33] assemblies of Herceptin are denoted as PEGx-HerNPs. Herceptin loading in 2-arm-PEG(600)-HerNP was approximately 9.65×10^4 Herceptin molecules per particle after template removal. FTIR spectroscopy confirmed the presence of PEG and Herceptin in the PEG*x*-HerNPs (Figure S1). TEM images show that PEG*x*-HerNPs had mean diameters ranging from 300 to 380 nm

(Figures 1A and S2). In comparison, the MSN templates had diameters of approximately 250 nm (Figure S3). The hydrodynamic size distributions measured by dynamic light scattering (DLS) in DPBS solution showed that with varying PEG arm length or arm number, the mean diameter of PEG*x*-HerNPs ranged from 250 to 350 nm (Figures 1B and S4). The thickness of the air-dried PEG*x*-HerNPs as measured by AFM varied from 80 to 150 nm (Figure S5), which indicates that the particles collapse upon drying. The ζ-potential of the PEG*x*-HerNPs increased from −17 to −4 mV with increasing PEG arm length (Figure 1C). The increase in the ζ-potential, which is related to the particle surface charge, indicates that the use of PEG with longer arm lengths or higher M_w results in particles with a near-neutral ζ-potential. The 2-arm-PEG(5k)-HerNPs exhibited the most neutral zeta potential value (−3.9 ± 6.5 mV) because it is cross-linked with a cross-linker with the longest arm length (M_w 5,000 g mol^{-1}) (Scheme 1). It is therefore expected to have the highest PEG/antibody ratio despite the multi-arm PEG having equal or higher M_w. No significant difference in the ζ-potential was found with the increase in PEG arm number. CD spectroscopy (Figure 1D) suggested that PEGylation, regardless of arm length or arm number, did not influence the molecular conformation of the antibody, as the PEG*x*-HerNPs maintained the same secondary structures as the free antibodies. This also indicates that treatment of the particles with HF (1 M) to remove the MSN template does not affect the secondary structure of the antibodies, which is in agreement with reported studies on HF-treated protein and protein-loaded particles.[41–44]

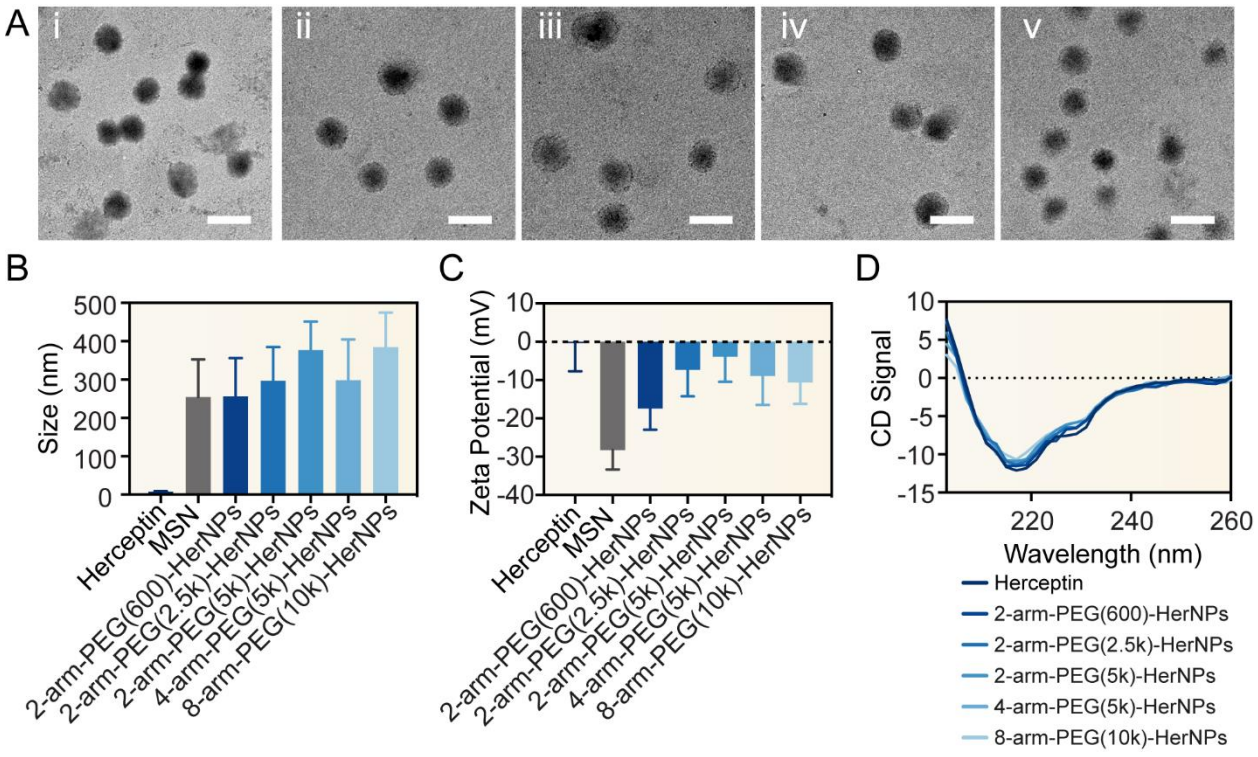

Figure 1. Characterization of PEG*x*-HerNPs cross-linked by various PEG linkers. (A) TEM images of PEG*x*-HerNPs cross-linked by (i) 2-arm-PEG(600), (ii) 2-arm-PEG(2.5k), (iii) 2-arm-PEG(5k), (iv) 4-arm-PEG(5k), or (v) 8-arm-PEG(10k). Scale bars: 500 nm. (B) Hydrodynamic size distributions of PEG*x*-HerNPs in DPBS solution as measured by DLS. Data are presented as mean ± standard deviation. (C) ζ-Potentials of PEG*x*-HerNPs measured in 2 mM phosphate buffer solution, pH 7.4. (D) CD spectra of PEG*x*-HerNPs.

Nanoparticle Stability. PEGylation of protein-loaded nanoparticles provides a steric barrier to prevent access to proteolytic enzymes and therefore protects the functional protein in the nanoparticles from degradation.[25] We previously reported that AbNPs, owing to their particulate form, accumulate intracellularly compared to free Ab, hence we sought to investigate the influence of PEGylation on the potential intracellular degradation of nanoparticles. The stability of PEG*x*-HerNPs in GSH and proteinase, which cause protein (disulfide bond) cleavage and protein

degradation, respectively, to mimic intracellular reducing and proteinase-rich conditions (in endo-lysosomes), was studied by SDS-PAGE, Figure 2A and 2B. After incubation in 5 mM of GSH (to simulate intracellular GSH concentration) for 24 h, the absence of protein fragments in the gel suggests that PEG*x*-HerNPs remained intact, whereas free Herceptin was separated into fragments via the cleavage of disulfide bonds, as supported by CD measurements (Figure S6). TEM images (Figure S7) confirmed that the PEG*x*-HerNPs remained in a particulate form with diameters consistent with those of untreated PEG*x*-HerNPs (200–400 nm). It is possible that disulfide bonds within the antibodies are cleaved by GSH but the strong cross-linking between PEG-NHS and the multiple amines on IgG, which typically has ~88 lysine residues or potentially reactive sites per IgG,[45] ensures that the antibody assembly remains relatively intact in a reducing environment.

When incubated in 1 mg mL^{-1} of proteinase for 24 h, both PEG*x*-HerNPs and free Herceptin were completely digested into smaller fragments (Figure 2B), showing the limited protection provided by PEG cross-linking when exposed to a proteinase-rich environment. To further understand the stability of the PEG*x*-HerNPs in a proteinase-rich environment, the degradation percentage of PEG*x*-HerNPs was quantified using AF488-labeled Herceptin antibodies. The AF488-labeled free Herceptin and PEG*x*-HerNPs were contained in dialysis tubing with a molecular weight cutoff of 100 kDa and incubated in 1 mg mL^{-1} of proteinase under gentle agitation. The initial total antibody amount of each sample was quantified by measuring the AF488 fluorescence intensity of each sample using a microplate reader. After incubation for 2, 4, 6, 8, 10, 24, or 48 h, the AF488-labeled antibody fragments that diffused out of the dialysis tubing were quantified using the same method. The percentage of degraded antibody fragments relative to the corresponding total antibody amount at various time points was calculated. The same experiment was conducted in DPBS (no proteinase) as control. The results showed that the PEG*x*-HerNPs

were more stable in proteinase than free Herceptin and as the PEG arm length or arm number increased, the PEG*x*-HerNPs became less susceptible to degradation (Figure 2C and 2D). Among all PEG cross-linkers studied, 8-arm-PEG(10k) provided the most effective protection to the antibodies from proteinase-induced degradation, resulting in only 30% of degradation after exposure to proteinase for 48 h. In contrast, over 90% of 2-arm-PEG(600)-HerNPs degraded under the same condition, while all PEG*x*-HerNPs remained stable and intact in DPBS (Figure S8). As indicated in the above results, different PEG cross-linkers provided varying degrees of protection to the antibodies within the nano-assemblies from proteolytic enzymes. PEG cross-linkers with a longer arm length and a higher arm number provided better protection possibly due to the thicker hydrated layer formed on the surface of the nanoparticles that sterically precluded the approach of proteolytic enzymes.[46,47]

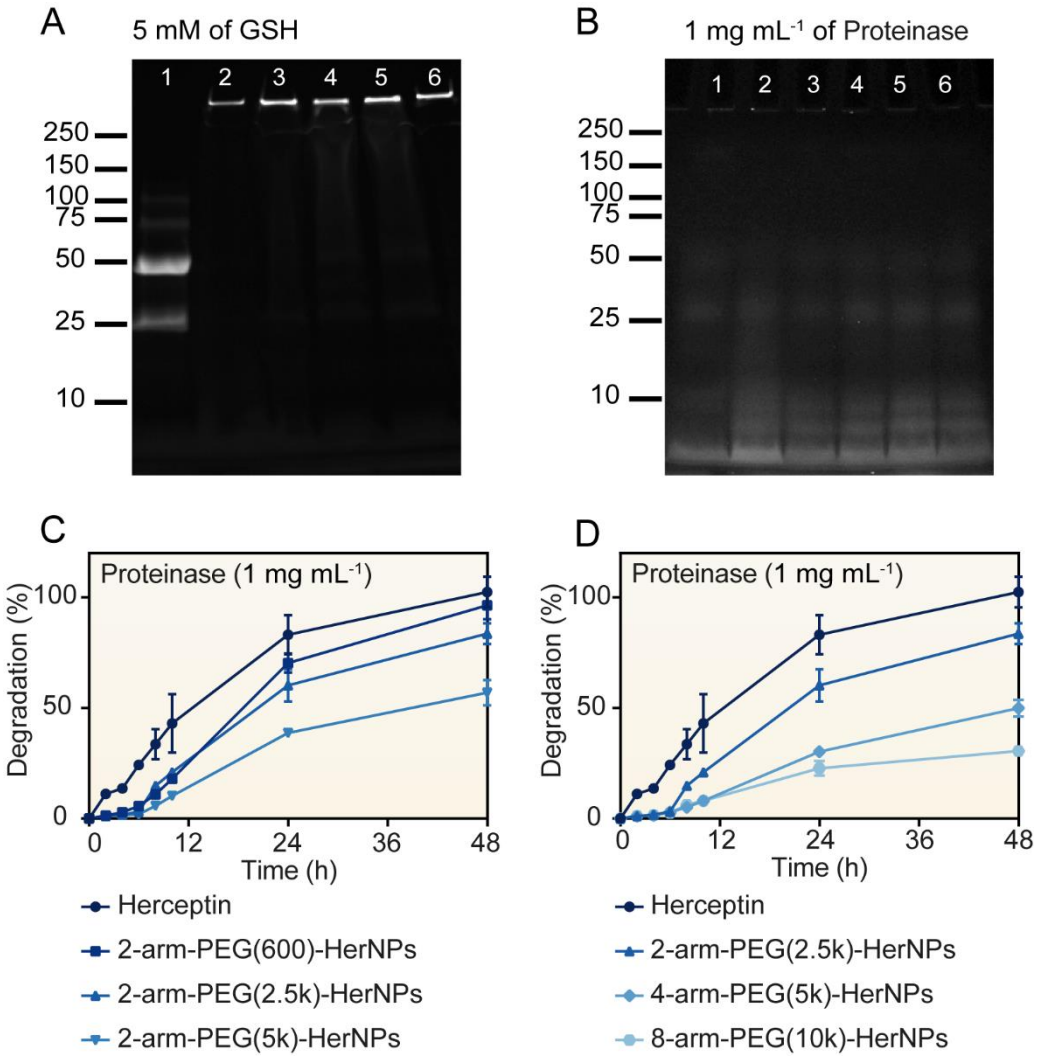

Figure 2. Stability of PEG*x*-HerNPs. Stability of PEG*x*-HerNPs in (A) 5 mM of GSH and (B) 1 mg mL^{-1} of proteinase after incubation for 24 h, as determined by SDS-PAGE: lane 1, Herceptin; lane 2, 2-arm-PEG(600)-HerNPs; lane 3, 2-arm-PEG(2.5k)-HerNPs; lane 4, 2-arm-PEG(5k)-HerNPs; lane 5, 4-arm-PEG(5k)-HerNPs; lane 6, 8-arm-PEG(10k)-HerNPs. Quantitative degradation profiles of PEG*x*-HerNPs cross-linked by PEG with (C) different arm lengths or (D) different arm numbers in 1 mg mL^{-1} of proteinase. Herceptin antibodies were labeled with AF488 for quantification.

Targeting Ability. The use of the model antibody Herceptin, which targets the ErbB2 receptor overexpressed in ~25% of invasive breast carcinomas,[48] enables the study of the functionality (targeting ability) of the PEG*x*-AbNPs. Herceptin has been complexed or conjugated to various macromolecules and used as a targeting ligand on diverse nanoparticle systems.[49–52] Herein, Herceptin serves as the functional building block in a particle assembly consisting only of protein and PEG (PEG*x*-HerNPs). The specific association of the PEG*x*-HerNPs to (ErbB2+) BT-474 breast cancer cells that overexpress ErbB2 was investigated by flow cytometry analysis. ErbB2− MDA-MB-231 breast cancer cells were used as control cells. The PEG*x*-HerNPs were incubated with ErbB2+ or ErbB2− cells in culture medium at 37 °C for 1, 3, 6, 12, or 24 h. The dosage was kept consistent at 20 μg mL^{-1} protein for all antibody and particle samples. 2-Arm-PEG(600)-IgGNPs, composed of IgG cross-linked by 2-arm-PEG(600), were also included as control (nontargeting) particles. Conjugation of AF488 dye to the antibody molecules prior to antibody assembly facilitated particle detection.

A flow cytometry study of binding kinetics showed that free Herceptin associated with BT-474 cells rapidly, whereas the PEG*x*-HerNPs associated with BT-474 cells in a time-dependent manner (Figures 3A, 3D and S9). Both the PEG arm length and arm number influenced the cell association of the PEG*x*-HerNPs to various degrees. Increasing the PEG arm length reduced the rate of cell association over 24 h (Figure 3A). However, after 24 h of incubation, all three PEG*x*-HerNP systems with different arm lengths, i.e., 2-arm-PEG(600)-HerNPs, 2-arm-PEG(2.5k)-HerNPs, and 2-arm-PEG(5k)-HerNPs, associated with over 90% of BT-474 cells, with nonsignificant difference among each particle system (Figure 3B). In contrast, a notable reduction in cell association percentage was observed with an increase in PEG arm number (Figure 3D). After 24 h of incubation, 2-arm-PEG(2.5k)-HerNPs, 4-arm-PEG(5k)-HerNPs, and 8-arm-PEG(10k)-HerNPs

associated to approximately 93%, 83%, and 74% of BT-474 cells, respectively (Figure 3E). These results suggest that increasing the PEG arm length limits the targeting ability of the nanoparticles within a short time frame (<24 h) but increasing the PEG arm number significantly hinders the targeting ability of the nanoparticles. A potential explanation is that the linear 2-arm-PEG is more flexible, leaving the receptor binding sites of the PEG*x*-HerNPs exposed, whereas the 4-arm- and 8-arm-PEG form a more rigid shield on the particle surface. Further characterization will be conducted in future studies to better understand the mechanism.

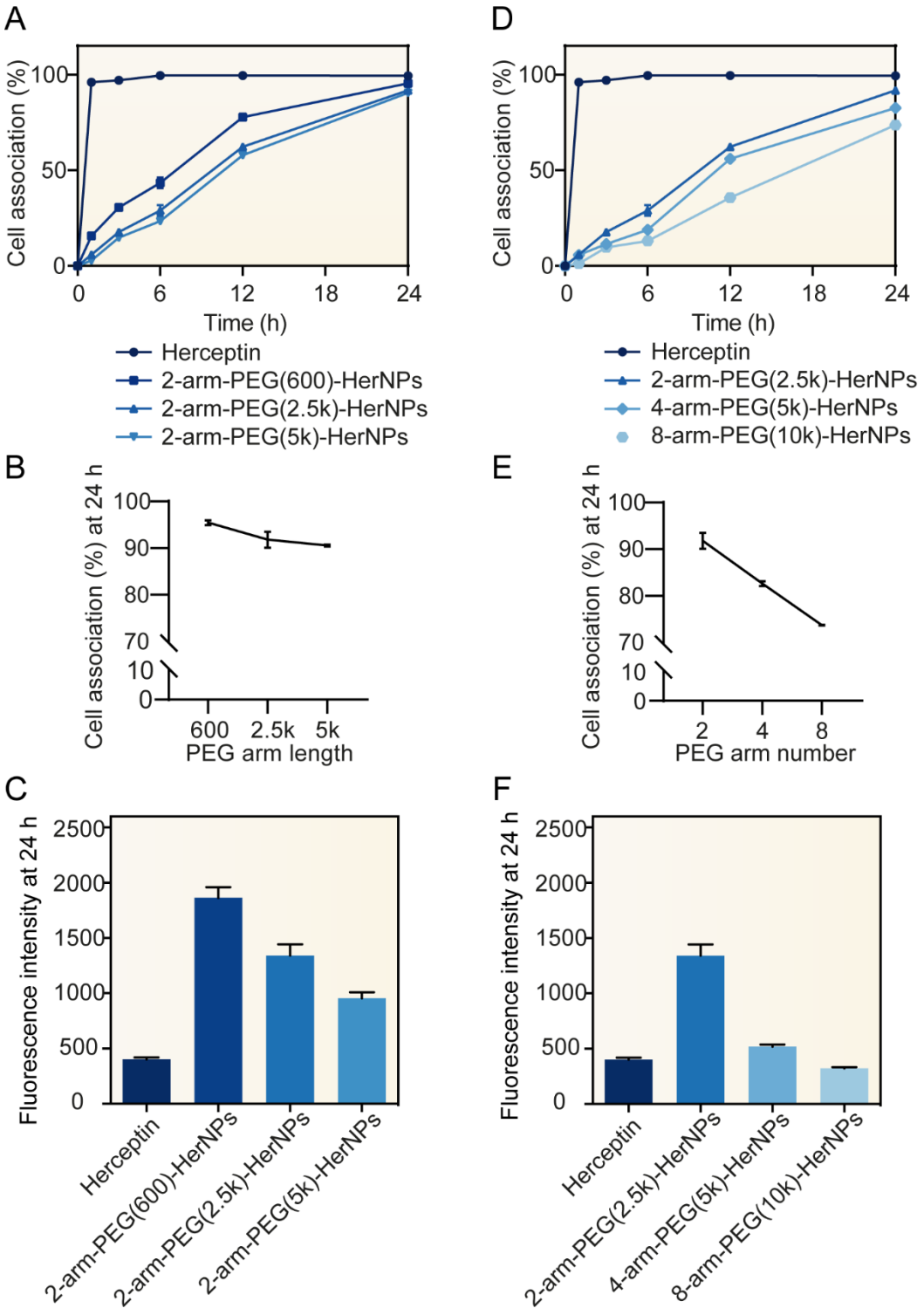

Figure 3. BT-474 cell association profiles of PEG*x*-HerNPs cross-linked by PEG with (A–C) different arm lengths or (D–F) different arm numbers, as measured by flow cytometry. Herceptin

antibodies were labeled with AF488 for detection. BT-474 cells were treated with the labeled Herceptin and PEG*x*-HerNPs at a dosage of 20 μg mL^{-1}. (A) and (D) Cell association (%) profiles of PEG*x*-HerNPs after incubation with BT-474 cells at different time points. (B) and (E) Cell association (%) after treatment for 24 h with PEG*x*-HerNPs. (C) and (F) AF488 fluorescence intensity of BT-474 cells after treatment with PEG*x*-HerNPs for 24 h. The cell fluorescence intensity profile is indicative of the number of antibodies associated with each cell.

In contrast to the association displayed to BT-474 cells, both free Herceptin and the PEG*x*-HerNPs had limited association with ErbB2− MDA-MB-231 cells (less than 5%, Figure S10). This result suggests that the PEG*x*-HerNPs retain the selective targeting ability of the Herceptin antibody molecules. Furthermore, the AF488 fluorescence intensity of the treated MDA-MB-231 and BT-474 cells was quantified as an indicator of the number of AF488-labeled antibodies associated with each cell. As expected, negligible fluorescence was detected in the treated MDA-MB-231 control cells (Figure S11), which further confirmed the specific targeting ability of the PEG*x*-HerNPs. In addition, the low nonspecific association of PEG*x*-HerNPs with MDA-MB-231 highlights the influence of PEGylation on reducing cell binding and uptake, which is consistent with our previous findings on PEG-based particles.[8,19] The fluorescence intensity of BT-474 cells treated with the PEG*x*-HerNPs for 24 h was significantly higher (up to 80%) than that of the cells treated with free Herceptin, which demonstrates that PEG*x*-HerNPs enabled more antibodies to associate with each target cell (Figure 3C and 3F). In addition, with the increase in PEG arm length from 600 Da to 5 kDa, the association intensity decreased by ~50% (Figure 3C). Similarly, increasing the PEG arm number from 2 to 8 resulted in a reduced cell fluorescence intensity of ~76% (Figure 3F). As the cell fluorescence intensity is indicative of the number of the antibodies

on the cell surface or inside the cells, tuning the PEGylation of the particles provides a potential strategy to control antibody accumulation in specific cells for therapeutic dosing.

Cellular Internalization. To investigate the effect of PEGylation on cellular uptake, the internalization of the PEG*x*-HerNPs in BT-474 cells was examined by imaging flow cytometry. After incubation with AF488-labeled PEG*x*-HerNPs for 24 h, cell membranes were stained with AF594-WGA and analyzed with an imaging flow cytometer, which captures individual bright-field and fluorescence images of each cell as the cells flow through the chamber. Based on the acquired images, the internalization of the PEG*x*-HerNPs was quantified by an internalization factor (IF) using the built-in internalization wizard of Amnis ImageStream IDEAS software based on the spatial relationship between the fluorescent nanoparticles and the cell membrane. A positive IF indicates internalized PEG*x*-HerNPs, whereas a negative IF indicates PEG*x*-HerNPs attached to the cell membrane.[53] The internalization percentage was calculated accordingly using the following formula: frequency of positive IF / frequency of both positive and negative IF × 100%. As shown in Figure 4, the internalization percentage values of the PEG*x*-HerNPs in BT-474 cells were all above 96%. All three 2-arm-PEG-HerNP systems exhibited a high internalization percentage (>99%) regardless of the PEG arm length (Figure 4A). As the PEG arm number increased from 2 to 8, the internalization percentage reduced slightly from 99% to 96%, as consistent with the reduction in AF488 fluorescence intensity (Figure 4B). The above results indicate that after 24 h incubation, the PEG*x*-HerNPs are mostly internalized inside the cells instead of remaining on the cell surface despite their different degrees of PEGylation. Hence, although there are fewer particles (and therefore antibodies) associated with cells as the PEG arm number increases as shown in Figure 3F, most of the cells (>96%) can internalize particles for intracellular delivery.

The internalization of the particles was further investigated by confocal laser scanning microscopy (CLSM). The cells were incubated with AF488-labeled PEG*x*-HerNPs for 24 h and then fixed with paraformaldehyde. AF488-labeled free Herceptin and IgGNPs were used as controls. From the microscopy images in Figure S12, the control IgGNPs were not observed inside BT-474 cells and free Herceptin was largely distributed on the cell membrane, as reported previously.[33] In contrast, the CLSM images in Figure 5 show that the PEG*x*-HerNPs are internalised by BT-474 cells, but the degree of internalization is dependent on the PEGylation. A larger amount of fluorescent 2-arm-PEG(600)-HerNPs were observed inside cells compared with 8-arm-PEG(10k)-HerNPs. The decreasing number of internalized PEG*x*-HerNPs as PEG arm length or arm number increases is consistent with the decreasing cell fluorescence intensity measured by flow cytometry (Figure 3C, F). However, despite the weak fluorescence signal from cells incubated with 8-arm-PEG(10k)-HerNPs for example (Figure 5), this still translates to positive association with BT-474 cells, albeit with fewer particles, as analyzed by flow cytometry (Figure 3D, E).

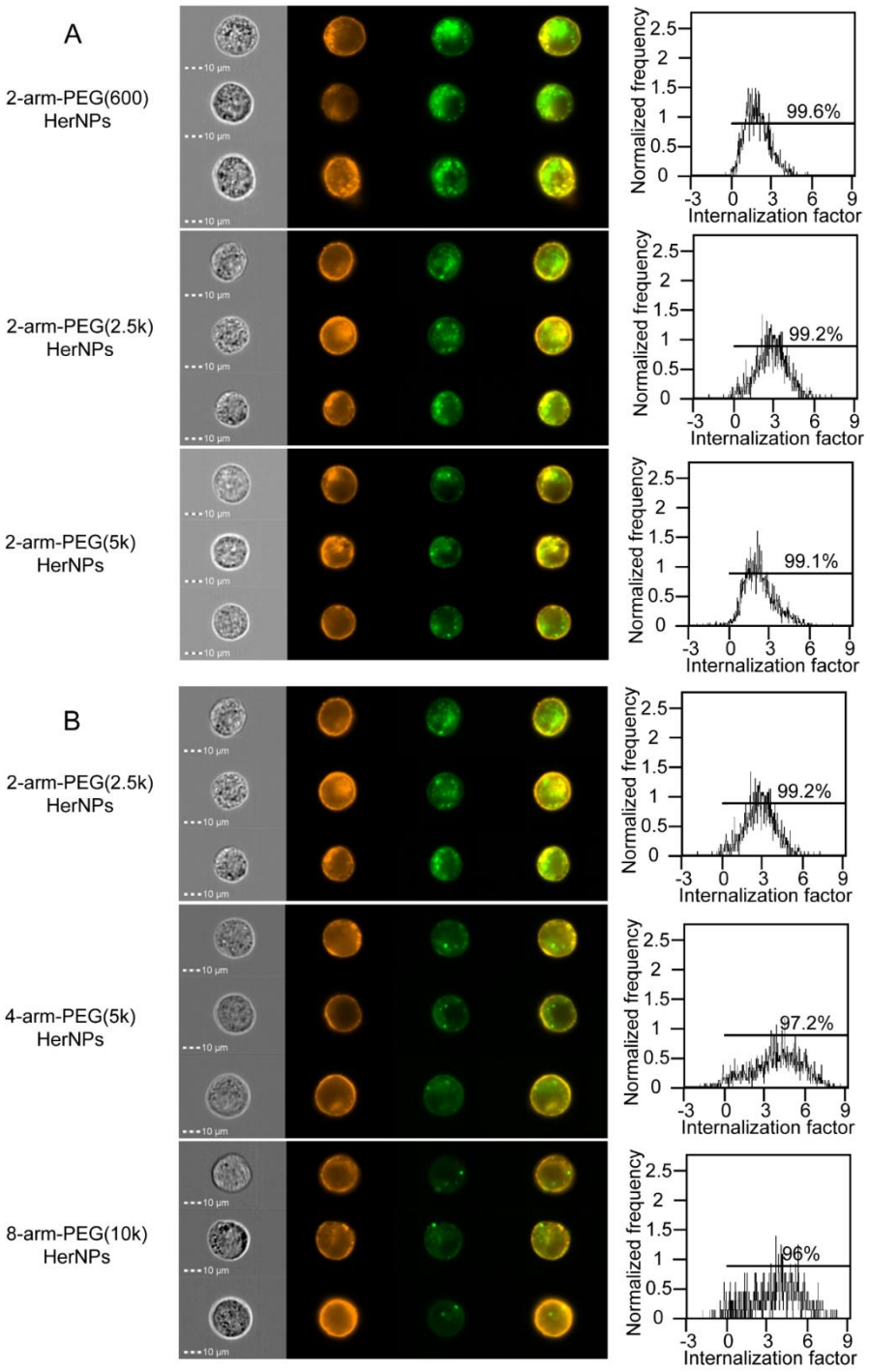

Figure 4. Cell internalization profiles of PEG*x*-HerNPs cross-linked by PEG linkers with (A) different arm lengths or (B) different arm numbers, as measured by imaging flow cytometry. BT-474 cells were incubated with PEG*x*-HerNPs (at 20 μg mL^{-1}) for 24 h at 37 °C. Cell membranes

were stained with AF594-WGA (orange) and Herceptin antibodies were labeled with AF488 (green) prior to particle assembly for imaging.

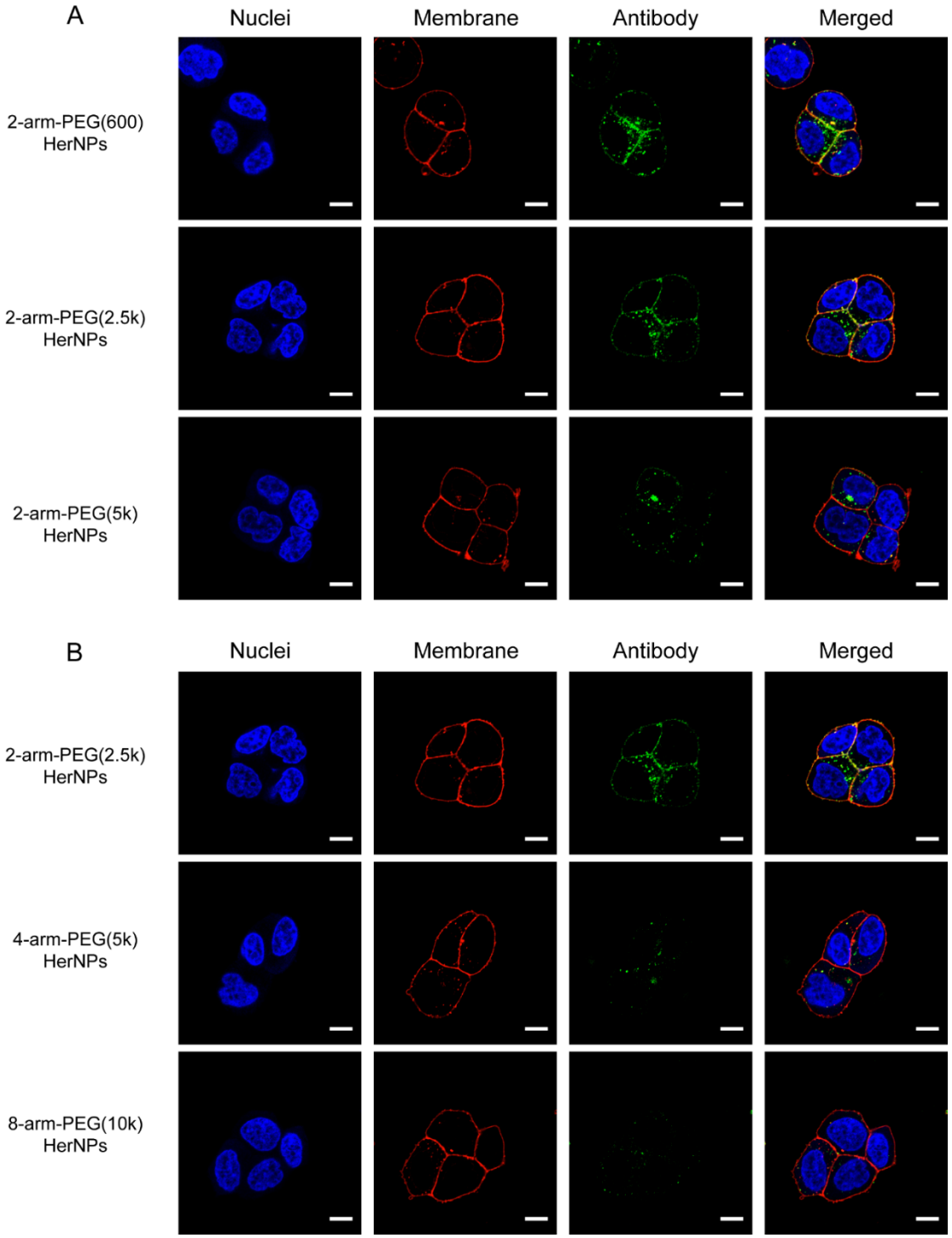

Figure 5. CLSM images of BT-474 cells treated with PEG*x*-HerNPs cross-linked by PEG with (A) different arm lengths or (B) different arm numbers. The cells were treated for 24 h at a dosage of 20 μg mL^{-1} before fixation. Nuclei were stained with Hoechst 33342 dye (blue); cell membrane was stained with AF594-WGA (red); Herceptin antibodies were labeled with AF488 (green). Scale bars: 10 μm.

Particle Functionality: Effect on Cell Proliferation. ErbB2 signaling is known to promote cell proliferation, which becomes uncontrolled in cancer. Herceptin interferes with ErbB2-triggered signaling by preventing ErbB2 receptor dimerization, which eventually inhibits cell proliferation.[54,55] To investigate the ability of the PEG*x*-HerNPs to limit cell proliferation, the proportion of viable ErbB2+ BT-474 cells and ErbB2− MDA-MB-231cells were examined by XTT assay after treatment with 20 μg mL^{-1} free Herceptin, 20 μg mL^{-1} PEGx-HerNPs, or cell culture medium (blank control) for 48 h at 37 °C. As observed from Figure 6, there was no reduction in cell viability in MDA-MB-231 cells after treatment with either of the particle systems studied, indicating that the PEG*x*-AbNPs are not toxic to nontarget cells. However, the PEG*x*-HerNPs could limit the proliferation (reduce cell viability) of the target BT-474 cells—for instance, the 2-arm-PEG(600)-HerNPs reduced cell viability by ~43% and at the same level as free Herceptin. This confirms that the PEG*x*-HerNPs retain the binding of the Herceptin antibodies to their receptor and prevent signaling. However, this functionality decreased as the PEG arm length increased. Specifically, as the PEG arm length increased from 600 Da to 5 kDa, cell viability increased from 57% to 78%, indicating that Herceptin displays reduced ability to bind to its receptor (Figure 6A). Similarly, increasing the PEG arm number from 2 to 8 limited receptor binding capability, as suggested by the increase in cell viability at higher arm numbers (>90%) (Figure 6B). A similar trend was observed when cells were treated with the PEG*x*-HerNPs at a

lower concentration (5 μg mL^{-1}, Figure S13). The effect of PEGylation on the growth inhibition functionality of the PEG*x*-HerNPs is consistent with the cellular association data, as growth inhibition is the downstream effect initiated by the binding of Herceptin antibodies to ErbB2 receptors on the cell membrane.

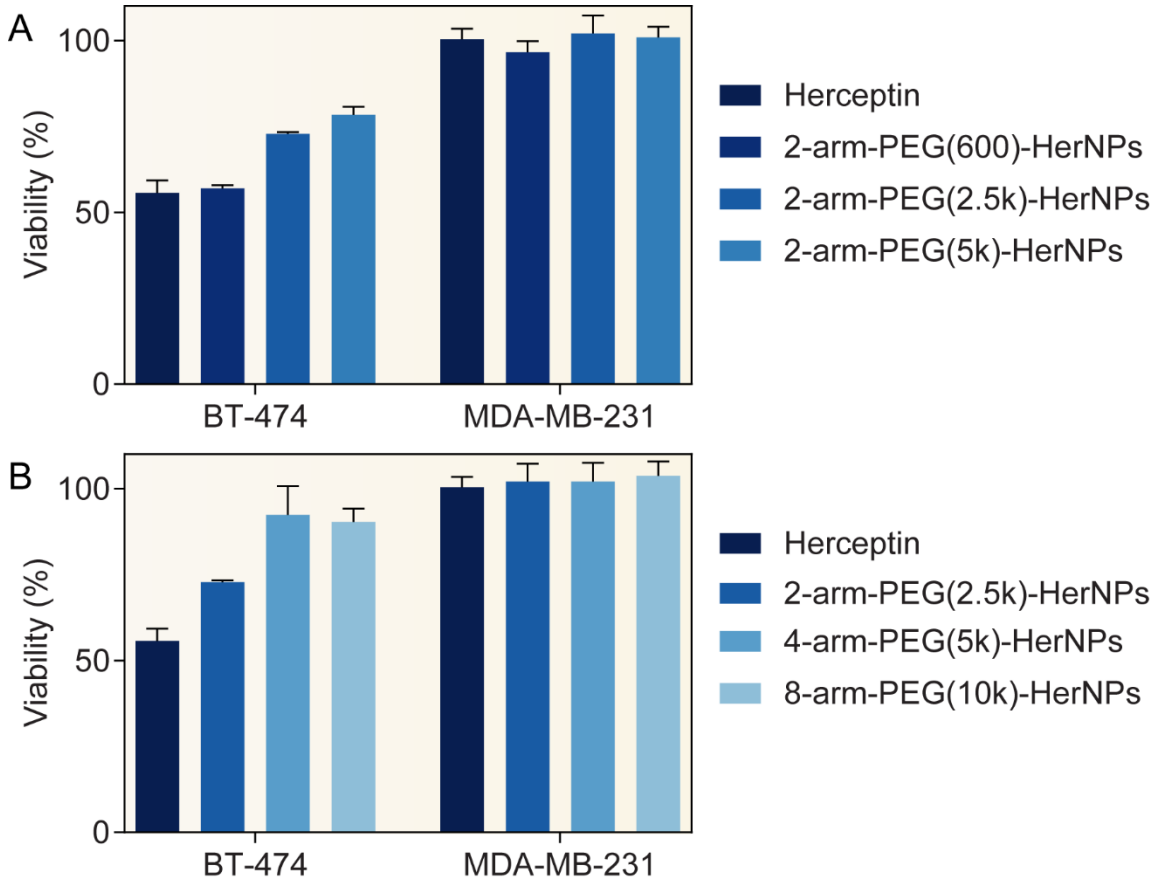

Figure 6. BT-474 and MDA-MB-231 cell growth inhibition of PEG*x*-HerNPs cross-linked by PEG with (A) different arm lengths or (B) different arm numbers, as determined by XTT assay. The cells were treated with free Herceptin or PEG*x*-HerNPs at an antibody concentration of 20 μg mL^{-1}. Cell viability was normalized against the viability of cell culture media-treated cells.

PEG*x*-HerNP Association with Phagocytes from Human Blood. A major obstacle to the efficacy of a targeted nanoparticle delivery system is the premature capture of the nanoparticles

by circulating leukocytes and mononuclear phagocytes, which causes their rapid clearance from the blood circulation and ultimately poor targeting.[56] To assess whether PEGylation can address this issue, the association of the PEG*x*-HerNPs with phagocytes in human whole blood was investigated using a previously developed human blood assay.[57] AF647-labeled PEG*x*-HerNPs were incubated in 100 μL of whole blood at 37 °C for 1 h. After the removal of red blood cells, the remaining cells were labeled with fluorophore-conjugated antibodies to identify distinct blood cell populations. Phagocytes, including dendritic cells, monocytes, and neutrophils, were identified and the association of the PEG*x*-HerNPs with these phagocytes was analyzed by multi-color flow cytometry. The results showed that <18% of dendritic cells, <10% of monocytes, and <2% neutrophils associated with the PEG*x*-HerNPs. With the increase in PEG arm length, the association of the PEG*x*-HerNPs with phagocytes decreased (Figure 7A i), whereas with the increase in PEG arm number, the association showed no statistically significant difference (Figure 7B i). The difference in PEG*x*-HerNP association with phagocytes could potentially be attributed to the formation of a biomolecular corona from the proteins and other biomolecules present in blood. Our previous studies have found that the corona compositions of PEG-based particles were affected by both PEG molecular structures and the plasma proteome of individual donors.[20,58] The level of specific antibodies (e.g., anti-PEG antibodies) in the plasma can also modulate the immune cell association with PEGylated nanoparticles.[59]

The association of the PEG*x*-HerNPs with lymphocytes (B cells, T cells, and NK cells) from human blood was also studied but there was negligible difference in cell association among the PEGylated assemblies (Figure S14). Using an in vitro phagocytic cell line, RAW 267.4 macrophages, cell association also decreased from 90% to 70% as the PEG arm length increased from 600 Da to 5 kDa (Figure 7A ii). When the PEG arm number increased from 2 to 4 and 8, the

association decreased further to 39% and 46%, respectively (Figure 7B ii). Overall, the 2-arm-PEG(5k)-HerNPs showed the lowest association with phagocytes in whole blood (Figure S15), whereas the multi-arm PEG*x*-HerNPs showed low association with phagocytic cells ex vivo and in vitro (Figure S16). The multi-arm PEG*x*-HerNPs, however, showed the lowest binding and internalization in target cells. Hence, careful consideration of the cross-linker is needed to balance both target cell-binding efficacy and avoiding phagocyte capture in blood circulation. It should be noted that the current assemblies use whole antibodies with the Fc portion of the antibodies present. As the antibodies are randomly oriented within the assemblies, it may be possible that some Fc fragments are exposed on the particle surface, which can enhance the immunogenicity of the particles. Although PEG cross-linking may shield the Fc fragments from immune cells, future work will also focus on particle assemblies of various antibody formats consisting of antigen binding fragments, including nanobodies and scFv.

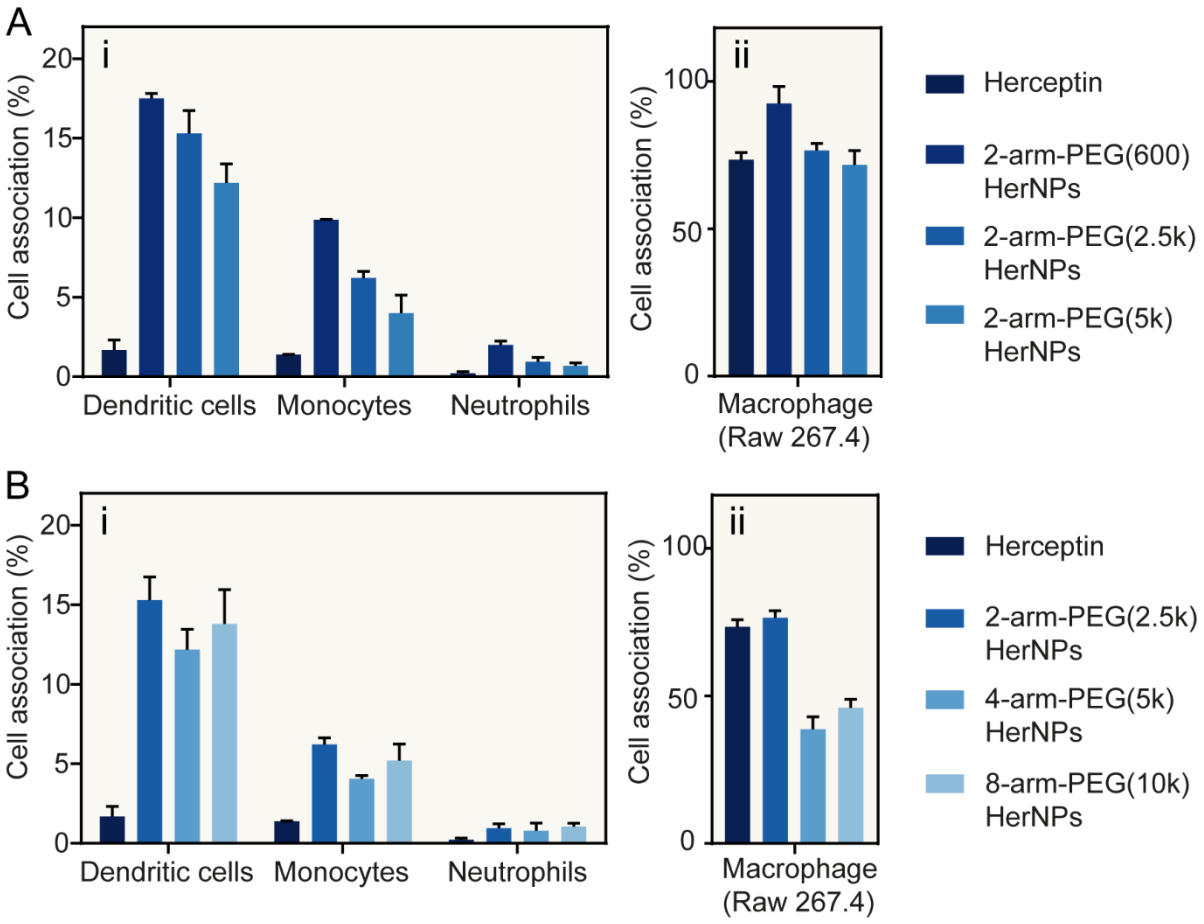

Figure 7. Phagocyte association of PEG*x*-HerNPs cross-linked by PEG with (A) different arm lengths or (B) different arm numbers. (i) Association of PEG*x*-HerNPs with phagocytic cells in human whole blood after incubation for 1 h, as quantified by flow cytometry. Herceptin antibodies were labeled with AF647. (ii) Association of PEG*x*-HerNPs with a macrophage (Raw 267.4) cell line in vitro after incubation for 24 h, as quantified by flow cytometry. Herceptin antibodies were labeled with AF488 for detection.

Biodistribution and Tumor Accumulation. The effect of PEG cross-linking on the in vivo biodistribution of the PEG*x*-HerNPs was assessed in mice (Figure 8). The antibodies were labeled with thulium (Tm) via a macrocyclic bifunctional chelator (*p*-SCN-Bn-DOTA). A study on the stability of Tm labeling, and hence the PEG*x*-HerNPs, in serum showed ~10% release of Tm from

PEG*x*-HerNPs after incubation for 24 h in serum (Figure S17). Tm-labeled free Herceptin and PEG*x*-HerNPs were injected intravenously in healthy BALB/c mice at a dosage of 10 mg mL^{-1}. The biodistribution of free Herceptin and PEG*x*-HerNPs at 4 h postinjection was qualitatively determined at the organ-level using inductively coupled plasma mass spectrometry (ICP-MS), which measures the Tm content of digested tissue preparations. Figure 8A shows that liver uptake of the PEG*x*-HerNPs decreases as the PEG arm length increases. Liver uptake, likely due to sequestration by Kupffer macrophages in the liver, is a major limitation impacting nanoparticle-mediated delivery efficacy.[60] A reduction in liver uptake could imply longer blood circulation of the particles. From the results in Figure 8A vi, an increase in the accumulation of PEG*x*-HerNPs with longer PEG arm lengths in blood was observed, indicating that 2-arm-PEG(5k)-HerNPs circulate longer than 2-arm-PEG(600)-HerNPs and 2-arm-PEG(2.5k)-HerNPs. The 2-arm-PEG(5k)-HerNPs also showed greater uptake in the kidney and heart. In contrast, in general, there was no significant difference in the biodistribution of the PEG*x*-HerNPs cross-linked with different PEG arm numbers (Figure 8B). Uptake in the spleen, another phagocyte-rich organ involved in particle clearance, was high for all particle systems (Figure 8A ii, 8B ii) although this was lower in 2-arm-PEG(5k)-HerNPs- and PEG(600)-HerNPs-treated mice. These results suggest that by varying the PEG cross-linker used to prepare PEG*x*-HerNPs, liver uptake can be tuned. The lower liver uptake and higher blood circulation of 2-arm-PEG(5k)-HerNPs, which could be due to their near-neutral ζ-potential (Figure 1C), make them the preferred PEG*x*-HerNP system to further investigate in vivo.

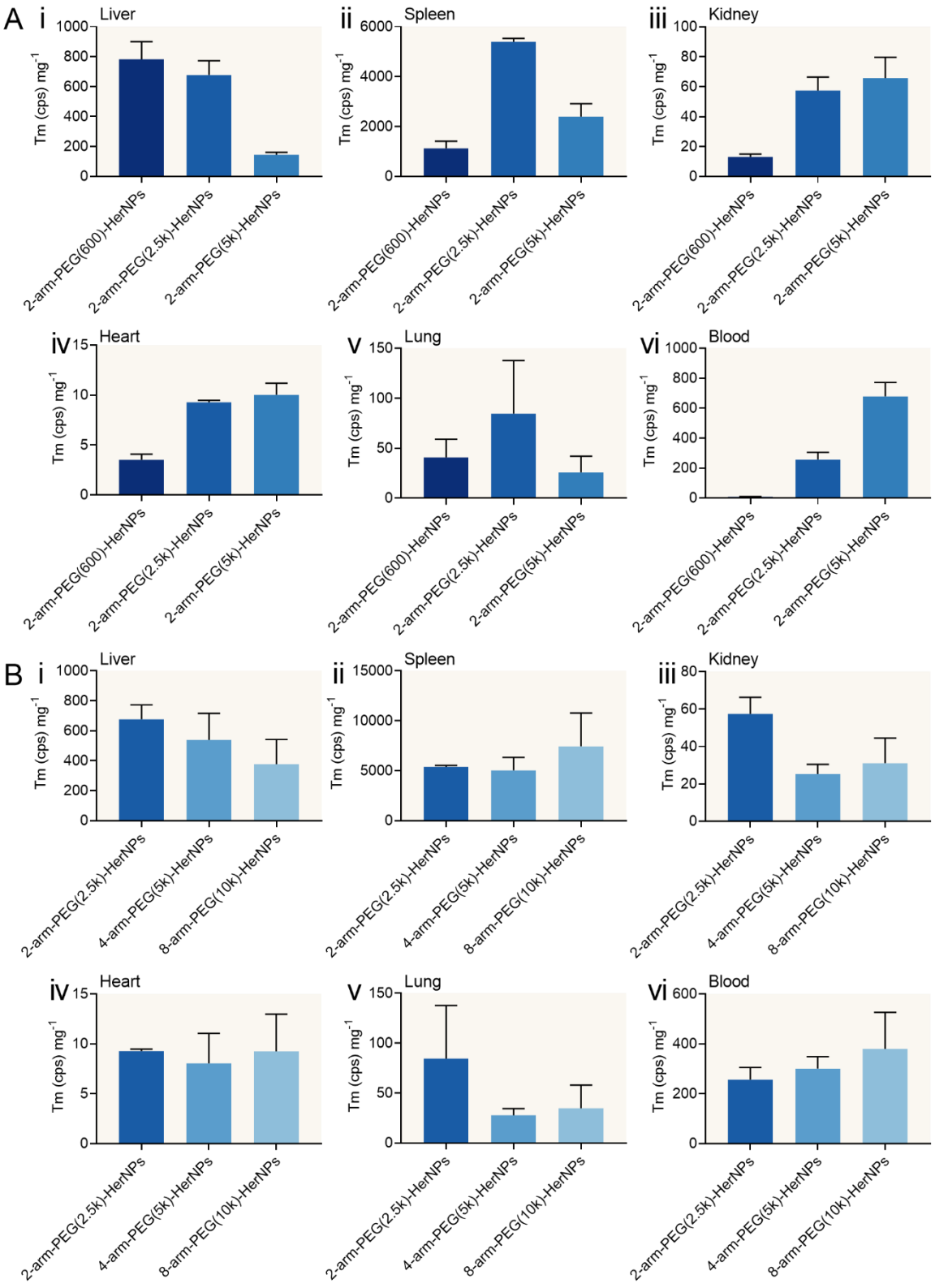
A
i
Liver
Tm (cps) mg-1
1000
800
600
400
200
0
2-arm-PEG(600)-HerNPs
2-arm-PEG(2.5k)-HerNPs
2-arm-PEG(5k)-HerNPs
ii
Spleen
6000
4000
2000
iii
Kidney
100
80
60
40
20
iv
Heart
15
10
5
v
Lung
150
100
50
vi
Blood
B
4-arm-PEG(5k)-HerNPs
8-arm-PEG(10k)-HerNPs
15000
10000
5000

Figure 8. In vivo biodistribution of Tm-labeled free Herceptin and PEG*x*-HerNPs cross-linked by PEG with (A) different arm lengths or (B) different arm numbers at 4 h postinjection in healthy BALB/c mice. The data are reported as Tm signal (counts per second, cps) per mg of tissue. Data represent means ± standard deviations based on triplicate samples.

To assess the capacity of 2-arm-PEG(5k)-HerNPs to target tumors (Figure 9A), radiolabeled particles were injected in BALB/c nu/nu mice bearing subcutaneous Erb2+ SK-OV-3 tumors. ^{64}Cu-labeled 2-arm-PEG(5k)-HerNPs were prepared via MeCOSar-NHS-ester ligands conjugated to Herceptin antibodies as described previously.[34] ^{64}Cu-labeled free Herceptin and 2-arm-PEG(5k)-IgGNPs were also prepared and injected as controls. The biodistribution of free Herceptin and the particles were qualitatively determined by PET/CT imaging. Figure 9 shows that at 24 h post administration, the highest antibody and particle accumulation were in the liver, which is typical even for targeted nanoparticle systems.[60] As expected, and as we showed previously,[33] there was higher tumor accumulation of free Herceptin than the particles, largely owing to their small size compared to particles (~370 nm, Figure 1B). Tumor uptake of 2-arm-PEG(5k)-HerNPs, however, was significantly higher (~50% higher) than that of the nontargeted 2-arm-PEG(5k)-IgGNPs (Figure 9B). These results suggest that the 2-arm-PEG(5k)-HerNPs retain their targeting capacity in vivo, even in a particulate form. Although the free antibody shows greater tumor accumulation than 2-arm-PEG(5k)-HerNPs, the ability to potentially target monoclonal antibody assemblies to tumors could be beneficial. In the current work and in our previous work, we show greater cell internalization of HerNPs than free antibody and previously demonstrated the use of a cleavable cross-linker to enable disassembly of IgGNPs under reductive conditions that mimic the internal cell environment.[33,61] Engineering AbNPs with a combination of cell surface and internal antigen targeting antibodies would have the potential to target and

modulate previously undruggable internal cancer targets. Reducing the size of the PEGylated HerNPs by using smaller templates, which is outside the scope of this work, could further improve their tumor targeting capacity in vivo. We expect that PEG*x*-AbNPs will be metabolized in vivo in the same way as monoclonal antibodies (i.e., metabolized into peptides and amino acids that can be re-used in the body or are excreted by the kidney). The PEG-NHS cross-linkers that are used have M_w's of less than 10,000 g mol^{-1}, which, upon antibody metabolism, are small enough to be cleared by kidney glomerular filtration.[62] Despite the availability of other low M_w NHS ester functional cross-linkers that could be used to cross-link the antibodies within HerNPs, PEG is already a clinically approved material and the wide range of PEG cross-linkers available that vary in M_w, architecture, and stimuli-responsiveness can be exploited to prepare AbNPs with tunable biological interactions for a range of applications, as demonstrated in this work.

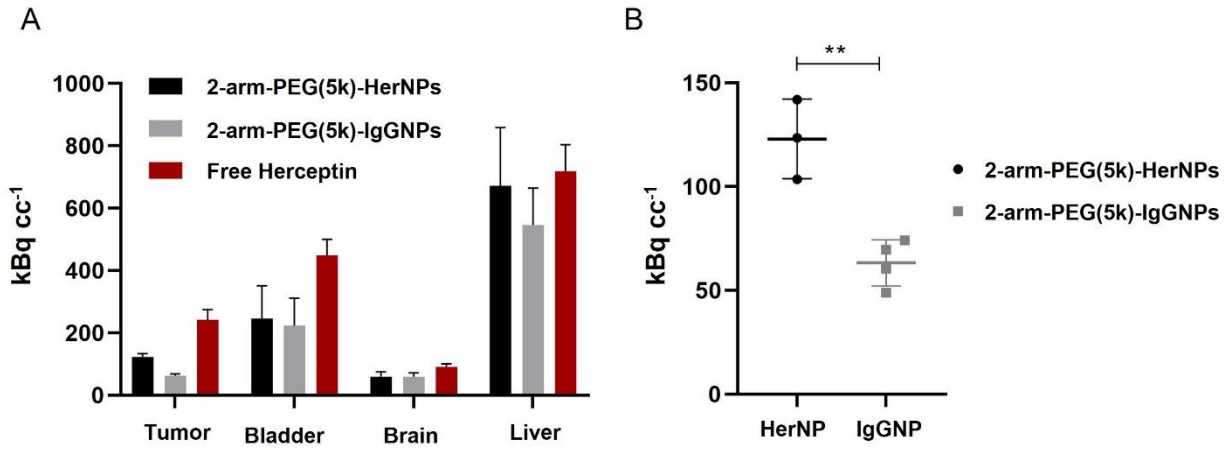

Figure 9. (A) In vivo biodistribution of ^{64}Cu-labeled 2-arm-PEG(5k)-HerNPs, 2-arm-PEG(5k)-IgGNPs, and free Herceptin at 4 h postinjection in SKOV3 tumor-bearing BALB/c nu/nu mice. The data are reported as kBq cc^{-1}. Data represent means ± standard deviations based on triplicate samples (n = 3–4). (B) *t*-test statistical analysis of the tumor targeting of 2-arm-PEG(5k)-HerNPs (n = 3) *versus* 2-arm-PEG(5k)-IgGNPs (n = 4). ** Indicates significant difference, $p < 0.01$.

CONCLUSIONS

This study demonstrates that nanoparticle engineering through nanoparticle cross-linking enables tunable bio–nano interactions at the in vitro to in vivo levels. PEGylated antibody nanoparticles (PEG*x*-AbNPs) composed of antibodies cross-linked by PEG with different arm lengths or arm numbers were used to study the effect of PEG cross-linking on the targeting ability, functionality (receptor blocking), phagocytic association, and in vivo biodistribution of the AbNPs. With increasing PEG arm length (from 600 Da to 5 kDa), the interaction of the PEG*x*-HerNPs with target cancer cells in vitro was consistently high (>90% at 24 h). Higher intracellular antibody accumulation and receptor binding (cytotoxicity) were observed for PEG*x*-HerNPs cross-linked by PEG with shorter arm lengths. However, the PEG*x*-HerNPs prepared using PEG with longer arms (higher M_w > 2.5 kDa) resulted in lower interaction with phagocytic cells that translated into up to 85% lower liver uptake in vivo. When multi-arm PEG was used as a cross-linker (4-arm and 8-arm), the interaction with target cells and antibody accumulation decreased with increasing arm number but the interaction with phagocytic cells in vitro and ex vivo were low. The results suggest that tuning AbNP efficacy requires balancing the targeting ability with potential premature in vivo clearance. Cross-linking particles with a linear PEG (i.e., 2 arm) but with longer or higher M_w arms (e.g., 2-arm-PEG(5k)-HerNPs) may achieve both reduced phagocytic capture and optimal targeting. In a tumor mouse model, 2-arm-PEG(5k)-HerNPs showed liver uptake at the same levels as free Herceptin and displayed 50% higher tumor accumulation than control AbNPs. While the deposition in the tumor was ~40% compared to free Herceptin, the increased intracellular delivery and the multifunctionality of the AbNP system combined with the potential for particle engineering provides opportunities for targeted combinatorial antibody assemblies optimized for their performance in vivo.

ASSOCIATED CONTENT

Supporting Information. FTIR spectra of PEG, Herceptin, and PEG*x*-HerNPs; size distribution of PEG*x*-HerNPs from TEM analysis; TEM image of the MSN templates; size distribution of MSN templates and PEG*x*-HerNPs using DLS; AFM analysis of PEG*x*-HerNPs; CD spectra of untreated and GSH-treated Herceptin; TEM images of GSH-treated PEG*x*-HerNPs; degradation kinetics of Herceptin and PEG*x*-HerNPs in proteinase; association kinetics of Herceptin, PEG*x*-HerNPs and 2-arm-PEG(600)-IgGNPs with BT-474 cells; association of Herceptin, PEG*x*-HerNPs and 2-arm-PEG(600)-IgGNPs with MDA-MB-231 cells at 24 h; fluorescence intensity of BT-474 and MDA-MB-231 cells after incubation with Herceptin and PEG*x*-HerNPs for 24 h; confocal microscopy images of BT-474 cells incubated with free Herceptin or IgGNPs for 24 h; viability of BT-474 and MDA-MB-231cells treated with Herceptin and PEG*x*-HerNPs for 24 h; association of Herceptin and PEG*x*-HerNPs with lymphocytes; association of Herceptin and PEG*x*-HerNPs with immune cells from human blood; association of Herceptin and PEG*x*-HerNPs with Raw 264.7 cells at 24 h; stability of Tm labeling; and MIRIBEL checklist for reporting research in bio–nano science. This material is available free of charge via the Internet at http://pubs.acs.org.

AUTHOR INFORMATION

Corresponding Author

*fcaruso@unimelb.edu.au

Author Contributions

The manuscript was written through contributions of all authors. All authors have given approval to the final version of the manuscript.

Notes

The authors declare no competing financial interest.

ACKNOWLEDGMENT

This research was conducted and funded by the Australian Research Council Centre of Excellence in Convergent Bio-Nano Science and Technology (project number CE140100036). F.C. acknowledges the award of a National Health and Medical Research Council (NHMRC) Senior Principal Research Fellowship (GNT1135806). C.E.H and F.C. acknowledge the award of a NHMRC Project Grant (GNT1138361) that also supported this work. F.C. and Y.J. acknowledge the award of an Australian Research Council Discovery Project (DP210103114) scheme that also supported this work. Y.J. acknowledges the award of an RMIT Vice Chancellor's Postdoctoral Fellowship. K.A. acknowledges the award of an NHMRC Career Development Fellowship (GNT1140465). This work was performed in part at the Materials Characterisation and Fabrication Platform (MCFP) at The University of Melbourne and the Victorian Node of the Australian National Fabrication Facility (ANFF). We thank Dr. Andrew Mitchell (MCFP) for his contribution in obtaining animal ethics approval.

REFERENCES

(1) Tavares, A. J.; Poon, W.; Zhang, Y. N.; Dai, Q.; Besla, R.; Ding, D.; Ouyang, B.; Li, A.; Chen, J.; Zheng, G. et al. Effect of Removing Kupffer Cells on Nanoparticle Tumor Delivery. *Proc. Natl. Acad. Sci. U. S. A.* **2017**, *114*, e10871–e10880.

(2) Liu, T.; Choi, H.; Zhou, R.; Chen, I. W. RES Blockade: A Strategy for Boosting Efficiency of Nanoparticle Drug. *Nano Today* **2015**, *10*, 11–21.

(3) Sun, X. L.; Yan, X. F.; Jacobson, O.; Sun, W. J.; Wang, Z. T.; Tong, X.; Xia, Y. Q.; Ling, D. S.; Chen, X. Y. Improved Tumor Uptake by Optimizing Liposome Based RES Blockade Strategy. *Theranostics* **2017**, *7*, 319–328.

(4) Liu, S.; Cheng, Q.; Wei, T.; Yu, X. L.; Johnson, L. T.; Farbiak, L.; Siegwart, D. J. Membrane-Destabilizing Ionizable Phospholipids for Organ-Selective mRNA Delivery and CRISPR-Cas Gene Editing. *Nat. Mater.* **2021**, *20*, 701–710.

(5) Cheng, Q.; Wei, T.; Farbiak, L.; Johnson, L. T.; Dilliard, S. A.; Siegwart, D. J. Selective Organ Targeting (SORT) Nanoparticles for Tissue-Specific mRNA delivery and CRISPR-Cas Gene Editing. *Nat. Nanotechnol.* **2020**, *15*, 313–320.

(6) Choi, H. S.; Ipe, B. I.; Misra, P.; Lee, J. H.; Bawendi, M. G.; Frangioni, J. V. Tissue- and Organ-Selective Biodistribution of NIR Fluorescent Quantum Dots. *Nano Lett.* **2009**, *9*, 2354–2359.

(7) Chertok, B.; Webber, M. J.; Succi, M. D.; Langer, R. Drug Delivery Interfaces in the 21st Century: From Science Fiction Ideas to Viable Technologies. *Mol. Pharm.* **2013**, *10*, 3531–3543.

(8) Cui, J. W.; De Rose, R.; Alt, K.; Alcantara, S.; Paterson, B. M.; Liang, K.; Hu, M.; Richardson, J. J.; Yan, Y.; Jeffery, C. M. et al. Engineering Poly(ethylene glycol) Particles for Improved Biodistribution. *ACS Nano* **2015**, *9*, 1571–1580.

(9) Wattendorf, U.; Merkle, H. P. PEGylation as a Tool for the Biomedical Engineering of Surface Modified Microparticles. *J. Pharm. Sci.* **2008**, *97*, 4655–4669.

(10) Harris, J. M.; Chess, R. B. Effect of Pegylation on Pharmaceuticals. *Nat. Rev. Drug Discovery* **2003**, *2*, 214–221.

(11) Howard, M. D.; Jay, M.; Dziublal, T. D.; Lu, X. L. PEGylation of Nanocarrier Drug Delivery Systems: State of the Art. *J. Biomed. Nanotechnol.* **2008**, *4*, 133–148.

(12) Karakoti, A. S.; Das, S.; Thevuthasan, S.; Seal, S. PEGylated Inorganic Nanoparticles. *Angew. Chem. Int. Ed.* **2011**, *50*, 1980–1994.

(13) Suk, J. S.; Xu, Q. G.; Kim, N.; Hanes, J.; Ensign, L. M. PEGylation as a Strategy for Improving Nanoparticle-Based Drug and Gene Delivery. *Adv. Drug Delivery Rev.* **2016**, *99*, 28–51.

(14) Ju, Y.; Cui, J. W.; Mullner, M.; Suma, T.; Hu, M.; Caruso, F. Engineering Low-Fouling and pH-Degradable Capsules through the Assembly of Metal-Phenolic Networks. *Biomacromolecules* **2015**, *16*, 807–814.

(15) Li, S. Y.; Ju, Y.; Zhou, J. J.; Noi, K. F.; Mitchell, A. J.; Zheng, T.; Kent, S. J.; Porter, C. J. H.; Caruso, F. Quantitatively Tracking Bio–Nano Interactions of Metal–Phenolic Nanocapsules by Mass Cytometry. *ACS Appl. Mater. Interfaces* **2021**, *13*, 35494–35505.

(16) Nance, E. A.; Woodworth, G. F.; Sailor, K. A.; Shih, T. Y.; Xu, Q. G.; Swaminathan, G.; Xiang, D.; Eberhart, C.; Hanes, J. A Dense Poly(ethylene glycol) Coating Improves Penetration of Large Polymeric Nanoparticles within Brain Tissue. *Sci. Transl. Med.* **2012**, *4*, 149ra119.

(17) Perrault, S. D.; Walkey, C.; Jennings, T.; Fischer, H. C.; Chan, W. C. W. Mediating Tumor Targeting Efficiency of Nanoparticles through Design. *Nano Lett.* **2009**, *9*, 1909–1915.

(18) Perry, J. L.; Reuter, K. G.; Kai, M. P.; Herlihy, K. P.; Jones, S. W.; Luft, J. C.; Napier, M.; Bear, J. E.; DeSimone, J. M. PEGylated PRINT Nanoparticles: The Impact of PEG Density on

Protein Binding, Macrophage Association, Biodistribution, and Pharmacokinetics. *Nano Lett.* **2012**, *12*, 5304–5310.

(19) Cui, J. W.; Bjornmalm, M.; Ju, Y.; Caruso, F. Nanoengineering of Poly(ethylene glycol) Particles for Stealth and Targeting. *Langmuir* **2018**, *34*, 10817–10827.

(20) Song, J.; Ju, Y.; Amarasena, T. H.; Lin, Z. X.; Mettu, S.; Zhou, J. J.; Rahim, M. A.; Ang, C. S.; Cortez-Jugo, C.; Kent, S. J. et al. Influence of Poly(ethylene glycol) Molecular Architecture on Particle Assembly and Ex Vivo Particle–Immune Cell Interactions in Human Blood. *ACS Nano* **2021**, *15*, 10025–10038.

(21) Li, S. Y.; Ju, Y.; Zhou, J. J.; Faria, M.; Ang, C. S.; Mitchell, A. J.; Zhong, Q. Z.; Zheng, T.; Kent, S. J.; Caruso, F. Protein Precoating Modulates Biomolecular Coronas and Nanocapsule–Immune Cell Interactions in Human Blood. *J. Mater. Chem. B* **2022**, *10*, 7607.

(22) Han, X. P.; Li, Z. B.; Sun, J.; Luo, C.; Li, L.; Liu, Y. H.; Du, Y. Q.; Qiu, S. H.; Ai, X. Y.; Wu, C. N. et al. Stealth CD44-Targeted Hyaluronic Acid Supramolecular Nanoassemblies for Doxorubicin Delivery: Probing the Effect of Uncovalent Pegylation Degree on Cellular Uptake and Blood Long Circulation. *J. Controlled Release* **2015**, *197*, 29–40.

(23) Ju, Y.; Cui, J. W.; Sun, H. L.; Mullner, M.; Dai, Y. L.; Guo, J. L.; Bertleff-Zieschang, N.; Suma, T.; Richardson, J. J.; Caruso, F. Engineered Metal-Phenolic Capsules Show Tunable Targeted Delivery to Cancer Cells. *Biomacromolecules* **2016**, *17*, 2268–2276.

(24) Roberts, M. J.; Bentley, M. D.; Harris, J. M. Chemistry for Peptide and Protein PEGylation. *Adv. Drug Delivery Rev.* **2012**, *64*, 116–127.

(25) Veronese, F. M. Peptide and Protein PEGylation: A Review of Problems and Solutions. *Biomaterials* **2001**, *22*, 405–417.

(26) Dos Santos, N.; Allen, C.; Doppen, A. M.; Anantha, M.; Cox, K. A. K.; Gallagher, R. C.; Karlsson, G.; Edwards, K.; Kenner, G.; Samuels, L. et al. Influence of Poly(ethylene glycol) Grafting Density and Polymer Length on Liposomes: Relating Plasma Circulation Lifetimes to Protein Binding. *Biochim. Biophys. Acta, Biomembr.* **2007**, *1768*, 1367–1377.

(27) He, Q. J.; Zhang, J. M.; Shi, J. L.; Zhu, Z. Y.; Zhang, L. X.; Bu, W. B.; Guo, L. M.; Chen, Y. The Effect of PEGylation of Mesoporous Silica Nanoparticles on Nonspecific Binding of Serum Proteins and Cellular Responses. *Biomaterials* **2010**, *31*, 1085–1092.

(28) Mori, A.; Klibanov, A. L.; Torchilin, V. P.; Huang, L. Influence of the Steric Barrier Activity of Amphipathic Poly(ethyleneglycol) and Ganglioside GM_1 on the Circulation Time of Liposomes and on the Target Binding of Immunoliposomes In Vivo. *FEBS Lett.* **1991**, *284*, 263–266.

(29) Cui, J. W.; Alt, K.; Ju, Y.; Gunawan, S. T.; Braunger, J. A.; Wang, T. Y.; Dai, Y. L.; Dai, Q.; Richardson, J. J.; Guo, J. L. et al. Ligand-Functionalized Poly(ethylene glycol) Particles for Tumor Targeting and Intracellular Uptake. *Biomacromolecules* **2019**, *20*, 3592–3600.

(30) Cui, J. W.; Ju, Y.; Houston, Z. H.; Class, J. J.; Fletcher, N. L.; Alcantara, S.; Dai, Q.; Howard, C. B.; Mahler, S. M.; Wheatley, A. K. et al. Modulating Targeting of Poly(ethylene glycol) Particles to Tumor Cells Using Bispecific Antibodies. *Adv. Healthcare Mater.* **2019**, *8*, 1801607.

(31) Saw, P. E.; Park, J.; Lee, E.; Ahn, S.; Lee, J.; Kim, H.; Kim, J.; Choi, M.; Farokhzad, O. C.; Jon, S. Effect of PEG Pairing on the Efficiency of Cancer-Targeting Liposomes. *Theranostics* **2015**, *5*, 746–754.

(32) Cruz, L. J.; Tacken, P. J.; Fokkink, R.; Figdor, C. G. The Influence of PEG Chain Length and Targeting Moiety on Antibody-Mediated Delivery of Nanoparticle Vaccines to Human Dendritic Cells. *Biomaterials* **2011**, *32*, 6791–6803.

(33) Hu, Y.; Li, J.; Ju, Y.; Houston, Z. H.; Fletcher, N. L.; De Rose, R.; Fernandes, S.; Hagemeyer, C. E.; Alt, K.; Thurecht, K. J. et al. Template-Assisted Antibody Assembly: A Versatile Approach for Engineering Functional Antibody Nanoparticles. *Chem. Mater.* **2022**, *34*, 3694–3704.

(34) Alt, K.; Paterson, B. M.; Ardipradja, K.; Schieber, C.; Buncic, G.; Lim, B.; Poniger, S. S.; Jakoby, B.; Wang, X. W.; O'Keefe, G. J. et al. Single-Chain Antibody Conjugated to a Cage Amine Chelator and Labeled with Positron-Emitting Copper-64 for Diagnostic Imaging of Activated Platelets. *Mol. Pharm.* **2014**, *11*, 2855–2863.

(35) Toth, G.; Szoor, A.; Simon, L.; Yarden, Y.; Szollosi, J.; Vereb, G. The Combination of Trastuzumab and Pertuzumab Administered at Approved Doses May Delay Development of Trastuzumab Resistance by Additively Enhancing Antibody-Dependent Cell-Mediated Cytotoxicity. *mAbs* **2016**, *8*, 1361–1370.

(36) Paterson, B. M.; Roselt, P.; Denoyer, D.; Cullinane, C.; Binns, D.; Noonan, W.; Jeffery, C. M.; Price, R. I.; White, J. M.; Hicks, R. J. et al. PET Imaging of Tumours with a ^{64}Cu Labeled Macrobicyclic Cage Amine Ligand Tethered to Tyr^3-Octreotate. *Dalton Trans.* **2014**, *43*, 1386–1396.

(37) Alt, K.; Paterson, B. M.; Westein, E.; Rudd, S. E.; Poniger, S. S.; Jagdale, S.; Ardipradja, K.; Connell, T. U.; Krippner, G. Y.; Nair, A. K. et al. A Versatile Approach for the Site-Specific Modification of Recombinant Antibodies Using a Combination of Enzyme-Mediated Bioconjugation and Click Chemistry. *Angew. Chem. Int. Ed.* **2015**, *54*, 7515–7519.

(38) Faria, M.; Bjornmalm, M.; Thurecht, K. J.; Kent, S. J.; Parton, R. G.; Kavallaris, M.; Johnston, A. P. R.; Gooding, J. J.; Corrie, S. R.; Boyd, B. J. et al. Minimum Information Reporting in Bio–Nano Experimental Literature. *Nat. Nanotechnol.* **2018**, *13*, 777–785.

(39) Yang, Y.; Bernardi, S.; Song, H.; Zhang, J.; Yu, M.; Reid, J. C.; Strounina, E.; Searles, D. J.; Yu, C. Anion Assisted Synthesis of Large Pore Hollow Dendritic Mesoporous Organosilica Nanoparticles: Understanding the Composition Gradient. *Chem. Mater.* **2016**, *28*, 704–707.

(40) Tan, Y. H.; Liu, M.; Nolting, B.; Go, J. G.; Gervay-Hague, J.; Liu, G.-y. A Nanoengineering Approach for Investigation and Regulation of Protein Immobilization. *ACS Nano* **2008**, *2*, 2374–2384.

(41) Greenberg, S.; Davies, P.; Schein, J.; Binder, L. Hydrofluoric Acid-Treated τ_{PHF} Proteins Display the Same Biochemical Properties as Normal *τ*. *J. Biol. Chem.* **1992**, *267*, 564–569.

(42) Yu, A.; Wang, Y.; Barlow, E.; Caruso, F. Mesoporous Silica Particles as Templates for Preparing Enzyme-Loaded Biocompatible Microcapsules. *Adv. Mater.* **2005**, *17*, 1737–1741.

(43) Mertz, D.; Wu, H.; Wong, J. S.; Cui, J.; Tan, P.; Alles, R.; Caruso, F. Ultrathin, Bioresponsive and Drug-Functionalized Protein Capsules. *J. Mater. Chem.* **2012**, *22*, 21434–21442.

(44) Städler, B.; Chandrawati, R.; Price, A. D.; Chong, S. F.; Breheney, K.; Postma, A.; Connal, L. A.; Zelikin, A. N.; Caruso, F. A Microreactor with Thousands of Subcompartments: Enzyme-Loaded Liposomes within Polymer Capsules. *Angew. Chem. Int. Ed.* **2009**, *48*, 4359–4362.

(45) Gautier, V.; Boumeester, A. J.; Lössl, P.; Heck, A. J. Lysine Conjugation Properties in Human IgGs Studied by Integrating High-Resolution Native Mass Spectrometry and Bottom-up Proteomics. *Proteomics* **2015**, *15*, 2756–2765.

(46) Miteva, M.; Kirkbride, K. C.; Kilchrist, K. V.; Werfel, T. A.; Li, H. M.; Nelson, C. E.; Gupta, M. K.; Giorgio, T. D.; Duvall, C. L. Tuning PEGylation of Mixed Micelles to Overcome Intracellular and Systemic siRNA Delivery Barriers. *Biomaterials* **2015**, *38*, 97–107.

(47) Owens, D. E.; Peppas, N. A. Opsonization, Biodistribution, and Pharmacokinetics of Polymeric Nanoparticles. *Int. J. Pharm.* **2006**, *307*, 93–102.

(48) Slamon, D. J.; Godolphin, W.; Jones, L. A.; Holt, J. A.; Wong, S. G.; Keith, D. E.; Levin, W. J.; Stuart, S. G.; Udove, J.; Ullrich, A. et al. Studies of the HER-2/Neu Proto-Oncogene in Human Breast and Ovarian Cancer. *Science* **1989**, *244*, 707–712.

(49) Chiu, S.-J.; Ueno, N. T.; Lee, R. J. Tumor-Targeted Gene Delivery Via Anti-HER2 Antibody (Trastuzumab, Herceptin®) Conjugated Polyethylenimine. *J Controlled Release* **2004**, *97*, 357–369.

(50) Chung, J. E.; Tan, S.; Gao, S. J.; Yongvongsoontorn, N.; Kim, S. H.; Lee, J. H.; Choi, H. S.; Yano, H.; Zhuo, L.; Kurisawa, M. et al. Self-Assembled Micellar Nanocomplexes Comprising Green Tea Catechin Derivatives and Protein Drugs for Cancer Therapy. *Nat. Nanotechnol.* **2014**, *9*, 907–912.

(51) Peng, J.; Chen, J.; Xie, F.; Bao, W.; Xu, H.; Wang, H.; Xu, Y.; Du, Z. Herceptin-Conjugated Paclitaxel Loaded PCL-PEG Worm-Like Nanocrystal Micelles for the Combinatorial Treatment of HER2-Positive Breast Cancer. *Biomaterials* **2019**, *222*, 119420.

(52) Juan, A.; Cimas, F. J.; Bravo, I.; Pandiella, A.; Ocaña, A.; Alonso-Moreno, C. An Overview of Antibody Conjugated Polymeric Nanoparticles for Breast Cancer Therapy. *Pharmaceutics* **2020**, *12*, 802.

(53) Shimoni, O.; Yan, Y.; Wang, Y. J.; Caruso, F. Shape-Dependent Cellular Processing of Polyelectrolyte Capsules. *ACS Nano* **2013**, *7*, 522–530.

(54) Arteaga, C. L.; Sliwkowski, M. X.; Osborne, C. K.; Perez, E. A.; Puglisi, F.; Gianni, L. Treatment of HER2-Positive Breast Cancer: Current Status and Future Perspectives. *Nat. Rev. Clin. Oncol.* **2012**, *9*, 16–32.

(55) Hudis, C. A. Trastuzumab — Mechanism of Action and Use in Clinical Practice. *New Engl. J. Med.* **2007**, *357*, 39–51.

(56) Vonarbourg, A.; Passirani, C.; Saulnier, P.; Benoit, J. P. Parameters Influencing the Stealthiness of Colloidal Drug Delivery Systems. *Biomaterials* **2006**, *27*, 4356–4373.

(57) De Rose, R.; Zelikin, A. N.; Johnston, A. P. R.; Sexton, A.; Chong, S. F.; Cortez, C.; Mulholland, W.; Caruso, F.; Kent, S. J. Binding, Internalization, and Antigen Presentation of Vaccine-Loaded Nanoengineered Capsules in Blood. *Adv. Mater.* **2008**, *20*, 4698–4703.

(58) Ju, Y.; Kelly, H. G.; Dagley, L. F.; Reynaldi, A.; Schlub, T. E.; Spall, S. K.; Bell, C. A.; Cui, J. W.; Mitchell, A. J.; Lin, Z. X. et al. Person-Specific Biomolecular Coronas Modulate Nanoparticle Interactions with Immune Cells in Human Blood. *ACS Nano* **2020**, *14*, 15723–15737.

(59) Ju, Y.; Lee, W. S.; Pilkington, E. H.; Kelly, H. G.; Li, S. Y.; Selva, K. J.; Wragg, K. M.; Subbarao, K.; Nguyen, T. H. O.; Rowntree, L. C. et al. Anti-PEG Antibodies Boosted in Humans by SARS-CoV-2 Lipid Nanoparticle mRNA Vaccine. *ACS Nano* **2022**, *16*, 11769–11780.

(60) Ngo, W.; Ahmed, S.; Blackadar, C.; Bussin, B.; Ji, Q.; Mladjenovic, S. M.; Sepahi, Z.; Chan, W. C. W. Why Nanoparticles Prefer Liver Macrophage Cell Uptake In Vivo. *Adv. Drug Delivery Rev.* **2022**, *185*, 114238.

(61) Lin, Y.; Chen, Z.; Hu, C.; Chen, Z. S.; Zhang, L. Recent Progress in Antitumor Functions of the Intracellular Antibodies. *Drug Discovery Today* **2020**, *25*, 1109.

(62) Ruggiero, A.; Villa C. H.; Bander, E.; Rey, D. A.; Bergkvist, M.; Batt, C. A.; Manova-Todorova, K.; Deen, W. M.; Scheinberg, D. A.; McDevitt, M. R. Paradoxical Glomerular Filtration of Carbon Nanotubes. *Proc. Natl. Acad. Sci. U. S. A.* **2010**, *107*, 12369–12374.

Table of Contents graphic